

## Article

# Paleoenvironmental Conditions and Factors Controlling Organic Carbon Accumulation during the Jurassic–Early Cretaceous, Egypt: Organic and Inorganic Geochemical Approach

Ahmed Mansour <sup>1</sup>, Thomas Gentzis <sup>2,\*</sup>, Ibrahim M. Ied <sup>3</sup>, Mohamed S. Ahmed <sup>4</sup> and Michael Wagreich <sup>5</sup>

<sup>1</sup> Geology Department, Faculty of Science, Minia University, Minia 61519, Egypt

<sup>2</sup> Core Laboratories, 6316 Windfern Road, Houston, TX 77040, USA

<sup>3</sup> Geology Department, Faculty of Science, Zagazig University, Zagazig 44519, Egypt

<sup>4</sup> Geology and Geophysics Department, College of Science, King Saud University, Riyadh 11451, Saudi Arabia

<sup>5</sup> Department of Geology, Faculty of Earth Sciences, Geography and Astronomy, University of Vienna, 1090 Vienna, Austria

\* Correspondence: thomas.gentzis@corelab.com

**Abstract:** The Jurassic–Early Cretaceous was a time of variable organic carbon burial associated with fluctuations of marine primary productivity, weathering intensity, and redox conditions in the pore and bottom water at paleo-shelf areas in north Egypt. This time interval characterized the deposition of, from old to young, the Bahrein, Khatatba, Masajid, and Alam El Bueib Formations in the north Western Desert. Although several studies have been devoted to the excellent source rock units, such as the Khatatba and Alam El Bueib Formations, studies on paleoenvironmental changes in redox conditions, paleoproductivity, and continental weathering and their impact on organic carbon exports and their preservation for this interval are lacking. This study presents organic and inorganic geochemical data for the Jurassic–Lower Cretaceous sediments from the Almaz-1 well in the Shushan Basin, north Western Desert. A total of 32 cuttings samples were analyzed for their major and trace elements, carbonates, and total organic carbon (TOC) contents. Data allowed the reconstruction of paleoenvironmental conditions in the southern Tethys Ocean and assessment of the changes in paleo-redox, paleo-weathering, and marine primary productivity, and the role of sediment supply. Additionally, factors that governed the accumulation of organic matter in the sediment were interpreted. Results showed that the Khatatba Formation was deposited during a phase of enhanced marine primary productivity under prevalent anoxia, which triggered enhanced organic matter production and preservation. During the deposition of the Khatatba Formation, significant terrigenous sediment supply and continental weathering were followed by a limited contribution of coarse clastic sediment fluxes due to weak continental weathering and enhanced carbonate production. The Bahrein, Masajid, and Alam El Bueib Formations were deposited during low marine primary productivity and prevalent oxygenation conditions that led to poor organic matter production and preservation, respectively. A strong terrigenous sediment supply and continental weathering predominated during the deposition of the Bahrein Formation and the lower part of the Alam El Bueib Formation compared to the limited coarse clastic supply and continental weathering during the deposition of the carbonate Masajid Formation and the upper part of the Alam El Bueib Formation. Such conditions resulted in the enhanced dilution and decomposition of labile organic matter, and, thus, organic carbon-lean accumulation in these sediments.

**Keywords:** redox conditions; marine primary productivity; continental weathering intensity; terrestrial clastic supply; organic matter preservation; carbonate dilution; Shushan Basin; north Western Desert



**Citation:** Mansour, A.; Gentzis, T.; Ied, I.M.; Ahmed, M.S.; Wagreich, M. Paleoenvironmental Conditions and Factors Controlling Organic Carbon Accumulation during the Jurassic–Early Cretaceous, Egypt: Organic and Inorganic Geochemical Approach. *Minerals* **2022**, *12*, 1213. <https://doi.org/10.3390/min12101213>

Academic Editor: Leszek Marynowski

Received: 13 August 2022

Accepted: 22 September 2022

Published: 26 September 2022

**Publisher's Note:** MDPI stays neutral with regard to jurisdictional claims in published maps and institutional affiliations.



**Copyright:** © 2022 by the authors. Licensee MDPI, Basel, Switzerland. This article is an open access article distributed under the terms and conditions of the Creative Commons Attribution (CC BY) license (<https://creativecommons.org/licenses/by/4.0/>).

## 1. Introduction

The Jurassic–Early Cretaceous is a time linked to a global icehouse and to warm greenhouse climate modes [1,2], and to intermittent occurrences of increased primary productivity, low oxygen (possibly anoxic) bottom water, and/or high burial and preservation rates of organic carbon [3–7]. Such major conditions were related to high atmospheric carbon dioxide gas emissions [1]. The north Western Desert is one of the major hydrocarbon provinces, mainly gas and oil, throughout the Egyptian territory, especially in the Shushan and Abu Gharadig Basins [4]. The Jurassic–Lower Cretaceous strata of the north Western Desert contain some intervals that are considered the main source rocks, such as in the Khatatba Formation [4–7] and, to some extent, in the Alam El Bueib Formation [4]. Although many geochemical studies for source rock assessment and the hydrocarbon generation potential of the Jurassic–Lower Cretaceous sediments have been carried out [5–9], studies into their inorganic (major and trace elements) and organic geochemical compositions and investigations into the paleoenvironmental redox conditions, marine paleoproductivity, role of terrigenous sediment supply, and continental weathering assessment are lacking.

In this study, the Jurassic–Lower Cretaceous strata from the Almaz-1 well (Figure 1) are represented, from old to young, by the Bahrein, Khatatba, Masajid, and Alam El Bueib Formations (Figure 2). Factors controlling the sedimentary organic carbon content during deposition comprise the positive impact of the production and preservation of organic matter that is characterized by episodes of organic carbon-rich facies compared to the negative influence of destruction via oxidation and/or organic matter dilution by high sedimentation rates and the deposition of organic carbon-lean sediments [10–14]. Although organic matter is easily decomposed, increased export productivity can partially intensify organic matter content in sediments delivered to the sediment–water interface and compensate its authigenic decomposition, especially at oxygen-depleted, stratified, and/or upwelling water column settings [12]. Quantification of total organic and inorganic carbon contents, as well as the analysis of major and trace elements can provide detailed information on the aforementioned paleoenvironmental variables. This includes redox conditions in the water column, pore and bottom waters, marine primary productivity, terrigenous clastic sediment fluxes, and climatic conditions and continental weathering. These environmental processes have a direct impact on organic matter diffusion and accumulation and, thus, the availability of organic carbon exports in the sediments [13].

In this study, an integrated approach to decipher various paleoenvironmental changes during the depositions of the Jurassic–Early Cretaceous in the Shushan Basin was conducted based on the investigation of trace element distributions and their relationship with total organic carbon (TOC) and carbonate contents. The aims of this study are to (1) interpret the paleo-redox conditions and role of marine primary productivity during the deposition of the Bahrein, Khatatba, Masajid, and Alam El Bueib Formations. This is significant to discriminate the organic carbon nature and distribution, and differentiate intervals dominated by organic carbon-rich sediments from those with organic carbon-poor sediments. (2) To assess the role of terrigenous coarse clastic sediment fluxes, and trends in continental weathering and paleoclimatic conditions during the depositions of the studied succession. These two objectives are essential to (3) assess the major controlling processes of organic carbon accumulation, especially for the commonly known organic carbon-rich sediments of the Middle Jurassic Khatatba Formation.

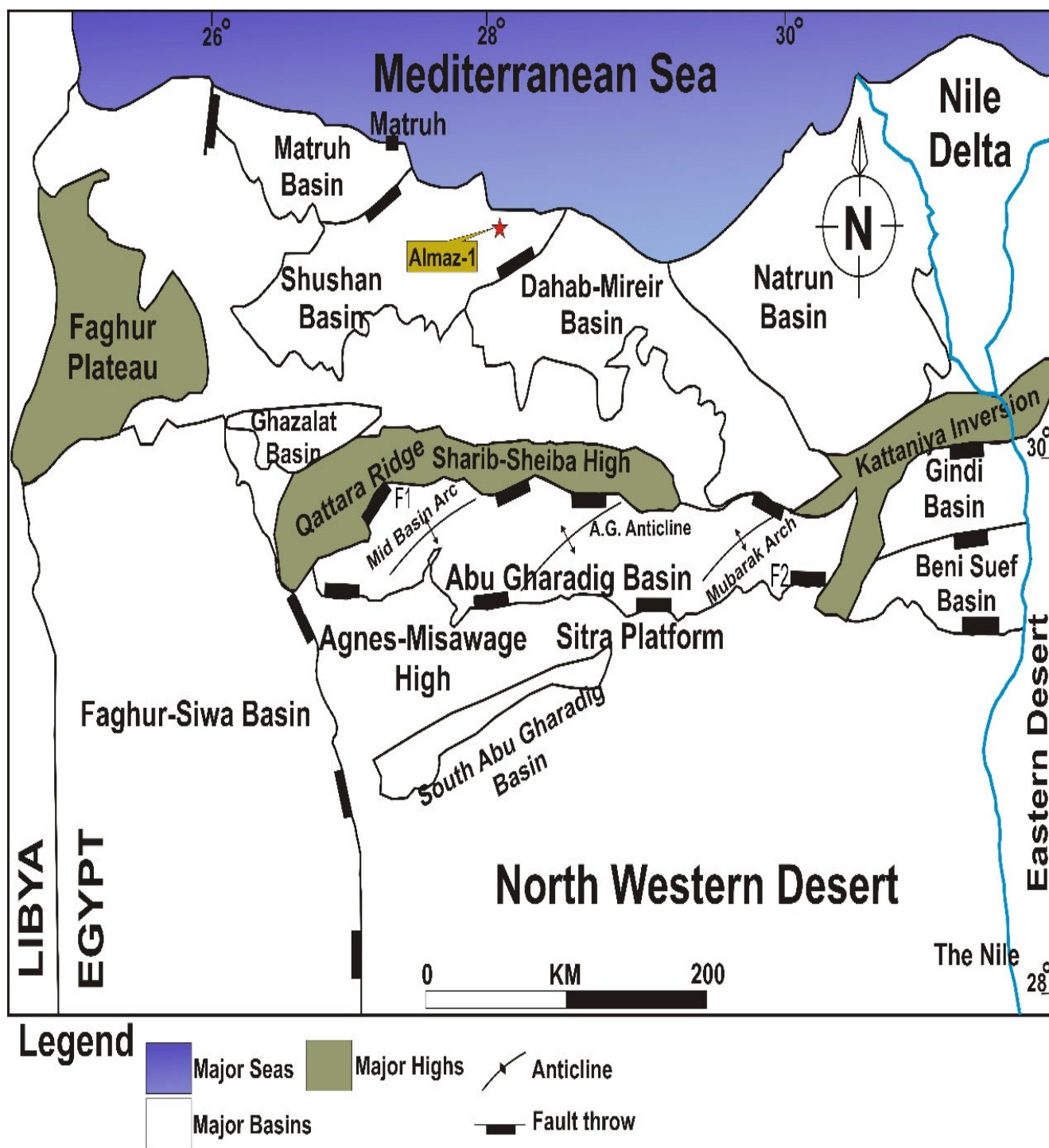


Figure 1. Location map of the Almaz-1 well (red star) along with major structural features in the north Western Desert, Egypt (modified after [4]).

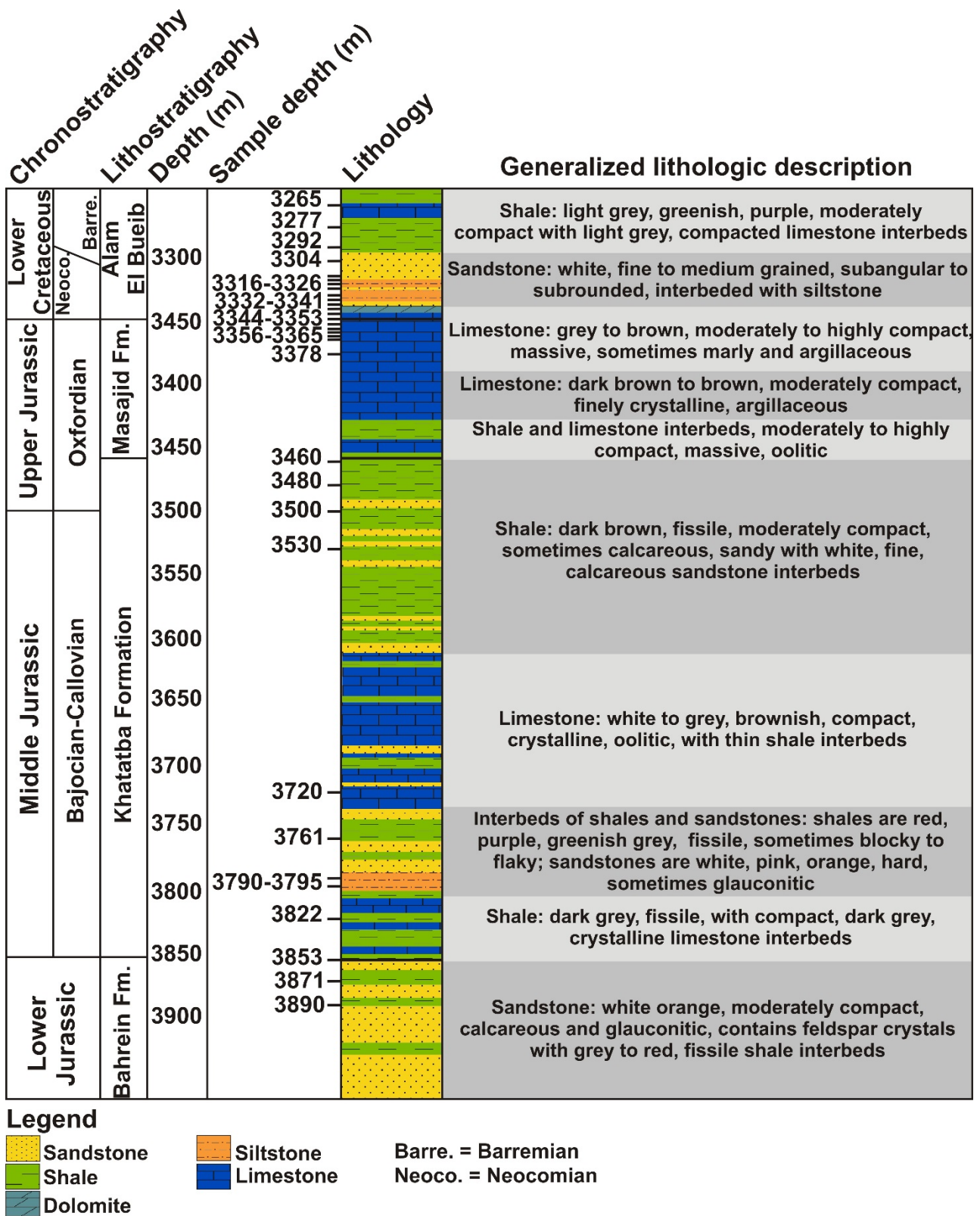


Figure 2. Lithostratigraphy and representative composite ditch cutting rock sample depths along with the generalized lithologic description of the Jurassic–Lower Cretaceous succession from the Almaz-1 well in the Shushan Basin, north Western Desert.

## 2. Regional Geology

### 2.1. Geologic Settings

The tectonic evolution of the Western Desert of Egypt was complex, especially the northern edge that contains coastal basins (i.e., the Natrun, Dahab-Mireir, Shushan, and Matruh Basins), which is an active structural area belonging to the unstable shelf [15,16]. The unstable shelf covers a large part of northern Egypt and represents an area with major transcontinental and regional fracture fault zones. Several rift basins in NE Africa developed in the Paleozoic in response to Pan-African orogenic events that led to the formation of fault zones that was followed by the onset of the Late Paleozoic Hercynian orogeny and related tectonic activities [15]. However, most of the basins in the Western Desert developed mainly during the Mesozoic (Jurassic–Cretaceous) [17]. In the Middle Jurassic, active spreading and rifting tectonism of the Central Atlantic and the development of the Alpine orogeny controlled the left-lateral drifting of north Africa and Europe [16,18–20]. The Alpine orogeny reached maximum activity during the Early Cretaceous and led to the development of NW–SE to WNW–ESE trending tensile stresses [20]. These conditions resulted in offshore deepening of the Tethys Ocean toward the south and the formation of the rift, sub-rift, and pull-apart basins in north Egypt. The pull-apart setting was the most prominent during the deposition of the Jurassic and Cretaceous thick stratigraphic successions in the Shushan Basin [4]. However, basin inversions and uplift tectonism took place during the late Turonian that were reported in northern basins of the Western Desert in response to a dextral drifting phase between Africa and Europe [21]. Further right-lateral movement of the African plate versus the European plate occurred during the late Santonian and generated NW-directed compressive forces, which triggered the formation of the Syrian Arc System in the northern and coastal basins of Egypt [15,16]. During the Campanian–Maastrichtian period, significant extensional forces and tectonic subsidence took place in NE Africa [20] at times of southern Tethys transgression, whereby most basins of the north Western Desert were subjected to deep marine setting and the deposition of chalky limestone facies [21].

The Shushan Basin is bounded by the Dahab-Mireir Basin to the east, the Matruh Basin and the Faghur-Umbarka Platform to the northwest and west, respectively, and the Qattara Ridge to the south (Figure 1). It has a thick stratigraphic succession that reaches at its maximum depocenter point to ca. 7600 m. It is described as a collapsed crest with NNE–SSW- and NE–SW-oriented inversion anticlines and tilted fault blocks that are bounded by NW–SE- and WNW–ESE-oriented normal faults [22].

### 2.2. Stratigraphic Settings

In the Shushan Basin, the stratigraphic succession of the Almaz-1 well comprised of Pre-Cambrian basement rocks, mainly fractured granitic rocks, followed by the Bahrein, Khatatba, Masajid, Alam El Bueib, Alamein Dolomite, Dahab Shale, Kharita, Bahariya, Abu Roash, and Khoman Formations. The current study focuses on the lower stratigraphic succession, represented by the Bahrein, Khatatba, Masajid, and Alam El Bueib Formations (Figure 2). The Lower Jurassic Bahrein Formation is composed of massive light pink to red and yellow colored, coarse-grained continental sandstone intercalated by thin layers of dark grey to red shale [4]. Due to local basement highs, the Bahrein Formation sometimes pinches out against the older Paleozoic rocks as is the case in the Almaz-1 well. The Bahrein Formation is conformably overlain by the Middle Jurassic Khatatba Formation. During the Bajocian–Kimmeridgian, a gradual rise in relative sea level in north Egypt took place and thick alternations between fine clastics and carbonates of the Khatatba and Masajid Formations were deposited. The Khatatba Formation consists of organic matter-rich black to brown shales interbedded with thin layers of white and pink hard sandstones. The middle part of the Khatatba Formation is represented by a thick interval of white to grey oolitic and argillaceous limestones with minor shale interbeds (Figure 2). The depositional paleoenvironment of the Khatatba Formation fluctuated between fluvio-deltaic and shallow marine conditions [5]. The Oxfordian–Kimmeridgian Masajid Formation

conformably overlies the Khatatba Formation. It is composed of a thick unit of grey to dark brown limestones, which are usually argillaceous at the base. The Masajid Formation was deposited in shallow marine to shelf basin conditions [4]. The Lower Cretaceous Alam El Bueib Formation rests conformably on the Masajid Formation. It consists of white to yellow sandstones and siltstones with consequent alternations of grey shales and compacted limestones. Carbonate facies are more common in the upper part of the Alam El Bueib Formation. This formation was deposited in a shallow marine shelf environment.

### 3. Material and Methods

Thirty-two (32) drill cuttings samples were taken from a thick stratigraphic succession (approximately 640 m thick, Figure 2) represented, from old to young, by the Bahrein, Khatatba, Masajid, and Alam El Bueib formations, respectively, in the Almaz-1 well. This exploratory well was drilled in the Shushan Basin of the northern part of the Western Desert by the Santa Fe 69 Oil Company (Dallas, TX, USA) in 1978. The Almaz-1 well is located at latitudes 30° 57' 06.01" N and longitudes 28° 23' 06.13" E (Figure 1).

#### 3.1. Total Organic Carbon (TOC) and Carbonate Analyses

All samples of the studied succession were measured for their TOC and carbonate contents. For TOC measurements, powdered samples were treated with HCl (25%) for 24 h to remove inorganic carbon. The residue was then washed with distilled water to remove HCl and dried at 50 °C for 1–2 h. Then, an aliquot (approximately 100 mg) of each powdered sample was measured using a LECO CS-200 carbon analyzer at 1100 °C in an induction furnace at Centre of Microbiology and Environmental Systems Science, University of Vienna. The analytical error after triplication was ±0.2 wt%.

The carbonate content was measured using the Müller-Gastner-Bomb devices [23] at the Department of Geology, University of Vienna. An aliquot of 65 mg of each powdered sample was digested in concentrated HCl (25%) and results were obtained directly in 10 s via the Müller-Gastner-Bomb.

#### 3.2. Major and Trace Element Measurements

The bulk geochemical composition of the current study samples (e.g., Al<sub>2</sub>O<sub>3</sub>, SiO<sub>2</sub>, CaO, MgO, MnO, Fe<sub>2</sub>O<sub>3</sub>, TiO<sub>2</sub>, K<sub>2</sub>O, P<sub>2</sub>O<sub>5</sub>, Cr<sub>2</sub>O<sub>3</sub>, Zr, Ni, V, Cu, Rb, Sr, Ba, Zn, and Pb) was measured using a modern machine of handheld energy-dispersive X-ray fluorescence at the Department of Geology, Faculty of Earth Sciences, Geography and Astronomy, University of Vienna, Austria. A total of 32 cuttings samples were powdered and placed in plastic cups. The bases of these cups were covered by thin plastic wrap (25 mm in diameter). For elemental measurements, each plastic cup was placed on top of a Bruker AXS TRACER IV-SD of the handheld machine equipped with a Rh X-ray tube with a beam pointing upward. All samples were subjected to dual mode measurements with two excitation energies (low- and high-energy) at 210 s for each phase. The low-energy phase measured major elements as well as Ni and V at 0.055 mA and 15 kV, whereas the high-energy phase was employed to measure the other trace elements at 0.0065 mA and 40 kV with an Al-Ti filter of 300 µm and 25 µm, respectively. The software SPECTRA<sup>EDX</sup> S2 CONFIGURATION was loaded into proprietary Bruker AXS calibration, and the reference calibration of each element was evaluated via comparison to the concentration of equivalent element calculated using baseline corrected peak heights and interelement slope from the energy-dispersive system. The analytical error after multiple measurements was in the range from 0.5% to 2% and the detection limit for trace elements concentration was 2 ppm.

Redox conditions in pore and bottom waters could be evaluated via the authigenic enrichment of redox-sensitive trace elements, such as V, Ni, Co, Cu, Zn, U, Cd, and Mo [24]. For reliable interpretations of paleo-redox conditions, enrichment factors (EF) of redox-sensitive trace elements of average shale were employed by normalizing elemental concentration to Al using the formula  $EF(x) = (X/Al)_{\text{sample}} / (X/Al)_{\text{average shale}}$  [25]. For a depleted element, an EF value is less than 1, whereas a detectable authigenic enrichment

characterizes an EF value in the range of 1–3 compared to the average shale concentration. EF values that exceed 3 and 10 are assigned for moderate to high authigenic enrichment, respectively [24].

The biogenic Ba ( $Ba_{bio}$ ) that is commonly used to characterize the role of marine primary productivity was calculated as follows

$$Ba_{bio} = \text{total Ba} - \text{total Al} \times (Ba/Al)_{detr}$$

where  $Ba_{bio}$  is the accumulated biogenic Ba concentration in the sediments;  $(Ba/Al)_{detr}$  is the detrital Ba/Al ratio of average crustal rocks that ranges between 0.0032 and 0.0046. A value of 0.0039 was used to calculate the  $Ba_{bio}$  content following the approach of Reitz et al. [26] and Schoepfer et al. [27].

### 4. Results

#### 4.1. Total Organic Carbon Concentration

Within the Almaz-1 well, the TOC content varies significantly with average values of 2.2 wt%. A substantial rise in TOC content is seen in the Middle Jurassic interval with the highest TOC values recorded within the Khatatba Formation that fall in the range of 0.5–17.4 wt% with average values being 3.7 wt% (Figure 3). The TOC content within the Masajid and Bahrein Formations is generally low to moderate and falls in the range of 0.4–1.7 wt% (0.9 wt% on average) and 0.5–1.0 wt% (0.8 wt% on average), respectively. The Lower Cretaceous Alam El Bueib Formation is characterized by moderate to high TOC content that fall in the range of 0.9–8.0 wt% (1.9 wt% on average).

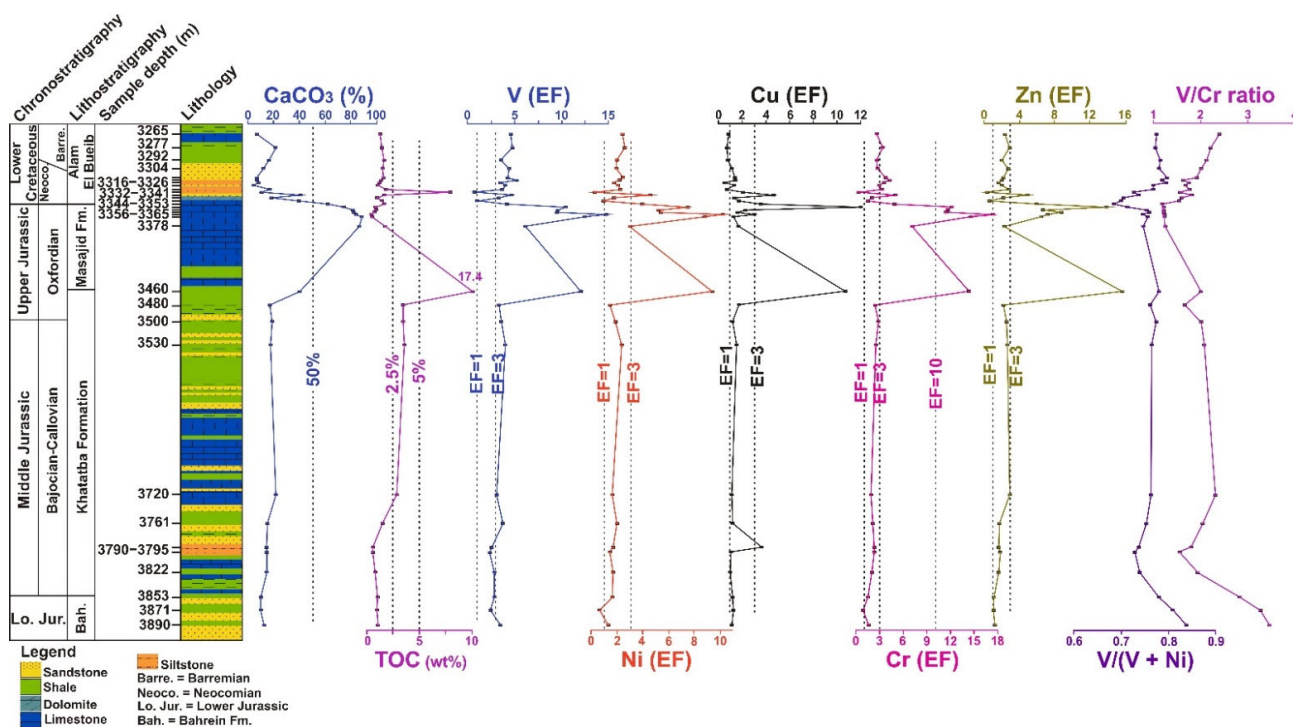


**Figure 3.** Chemostratigraphic distribution of TOC and enrichment factors of redox-sensitive trace elements and ratios of V/(V + Ni) of the Jurassic–Lower Cretaceous sediments from the Almaz-1 well, Shushan Basin. The V/(V + Ni) and V/Cr ratios were smoothed with a 3-point moving average.

#### 4.2. Carbonate Content

As with the TOC content, the carbonate content varies significantly within the studied succession, with values in the range of 4.8%–89.2%. The highest  $CaCO_3$  content is recorded within the Oxfordian Masajid Formation that reaches up to 89.2 wt% with an average

value of 80.3% (Figure 3). The Middle Jurassic Khatatba Formation is dominated by low to moderate carbonate content that is in the range from 14.9% to 40.5% (19.8% on average), whereas the Bahrein Formation is characterized by low carbonate content (9.1–12.7%, 10.4% on average). The lowest carbonate content occurs within the Lower Cretaceous Alam El Bueib Formation (4.8%–41.8%, 16.2% on average).

#### 4.3. Redox Proxies

The role of paleo-redox conditions was assessed for the studied Jurassic–Lower Cretaceous interval based on stratigraphic variations in enrichment factors of redox-sensitive trace elements, including V, Ni, Cr, Cu, and Zn (Supplementary Materials Table S1). Additionally, the redox proxy  $V/(V + Ni)$  was used to reveal prevalent oxygenation levels during deposition. Generally, the stratigraphic trends in the EFs of V, Ni, Cr, Cu, and Zn are markedly similar to each other and to the TOC profile (Figure 3). The Bahrein Formation at the lower part of the succession is characterized by low values of V, Ni, Cr, Cu, and Zn enrichment factors, which are in the range of 2.1–3.3 (avg. 2.7), 0.7–1.7 (avg. 1.2), 0.8–1.5 (avg. 1.24), 1.1–1.2 (avg. 1.1), and 1–1.2 (avg. 1.1), respectively. The values of the  $V/(V + Ni)$  and  $V/Cr$  ratios are the highest within the Bahrein Formation and are in the range of 0.75–0.83 and 2.6–4, respectively (Figure 3).

The Khatatba Formation is dominated by slightly higher average values of redox-sensitive element EFs that reach two- and three-times the average values of the Bahrein Formation. The highest values in the EFs of 15.6 and 14.3 are assigned to Zn and Cr, respectively, which occur at the topmost part of the Khatatba Formation.  $V_{EF}$ ,  $Ni_{EF}$ , and  $Cu_{EF}$  of the Khatatba Formation fall in the range of 2.1–11.9 (avg. 4.0), 1.5–9.4 (avg. 2.6), and 0.9–10.6 (avg. 2.5), respectively, whereby their highest values are consistent with the maximum TOC content at a depth of 3460 m (Figure 3). The  $V/(V + Ni)$  and  $V/Cr$  ratios exhibit a gradual fall at the lowermost part of the Khatatba Formation that are followed by a minor rise at the top with values in the range of 0.71–0.8 and 1.4–2.5, respectively (Figure 3).

In the carbonate Masajid Formation, variable EFs of 4.9–17.6, 4.0–14.9, 3.0–10.3, 1.3–12, and 2.3–13.7 are observed for the redox-sensitive trace elements Cr, V, Ni, Cu, and Zn, respectively. Enrichment factors for the former trace elements are more enriched in this interval compared to the Khatatba Formation (Figure 3). The  $V/(V + Ni)$  ratio shows a significant fall within the Masajid Formation from 0.8 to 0.65 that is followed directly by a long-term rise within the Alam El Bueib Formation from 0.65 to 0.82. Moreover, the  $V/Cr$  ratio is generally low within the Masajid Formation and ranges between 1.18 and 1.23 compared to a long-term increase within the Alam El Bueib Formation from 1.2 to 2.6 (Figure 3). The Lower Cretaceous Alam El Bueib Formation is characterized by low to moderate abundances of  $V_{EF}$ ,  $Ni_{EF}$ ,  $Cu_{EF}$ ,  $Zn_{EF}$ , and  $Cr_{EF}$  that are in the range of 0.7–5.1 (avg. 3.6), 0.4–4.5 (avg. 2.1), 0.6–4.6 (avg. 1.4), 0.2–4.9 (avg. 2.2), and 0.6–5.0 (avg. 2.9), respectively.

Additionally, Al-normalized redox-sensitive trace elements, including V, Ni, Cu, and Zn were plotted versus TOC content to provide further information on controlling mechanisms of their enrichment and thus deduce a reliable assessment of redox conditions during the depositions of the studied succession (Figure 4A). The high TOC samples of the Khatatba Formation show significant correlations between TE/Al and TOC relationships compared to the TOC-lean Bahrein, Masajid, and Alam El Bueib formations (Figure 4B–D).

#### 4.4. Paleoproductivity Proxies

The concentrations and behavior of specific TE/Al, such as Ba, Ni, Zn, and Cu, are commonly used to assess the role of marine biological productivity (Figure 5). The stratigraphic trends in Zn/Al, Ni/Al, and Cu/Al are significantly similar to the TOC profile (Figure 5, Table S1). Values of Zn/Al, Ni/Al, and Cu/Al substantially increase in the range of 10.2–166.8, 5.4–72.4, and 5.4–54.3, respectively, toward the topmost part of the Khatatba Formation. The  $Ba_{bio}$  shows two major peaks at the lower and uppermost

parts of the Khatatba Formation with average values of 636 and 308 ppm, respectively. The organic carbon-poor Masajid Formation shows significant variations toward high values in the ratios of Zn/Al (25.1–145, 77.8 on average), Ni/Al (23.0–79.2, 49.0 on average), and Cu/Al (6.4–61.2, 18.4 on average). It is dominated by the lowest concentration in the  $Ba_{bio}$  throughout the studied section (0 to 26 ppm, 8 ppm on average). Despite the occurrence of short-term peaks in Zn/Al, Ni/Al, and Cu/Al ratio within the lower part of the Alam El Bueib Formation, gradual long-term declines in these ratios are recorded toward the top (Figure 5). The  $Ba_{bio}$  in the Alam El Bueib Formation shows successive short-term oscillations with an average value of 206 ppm.

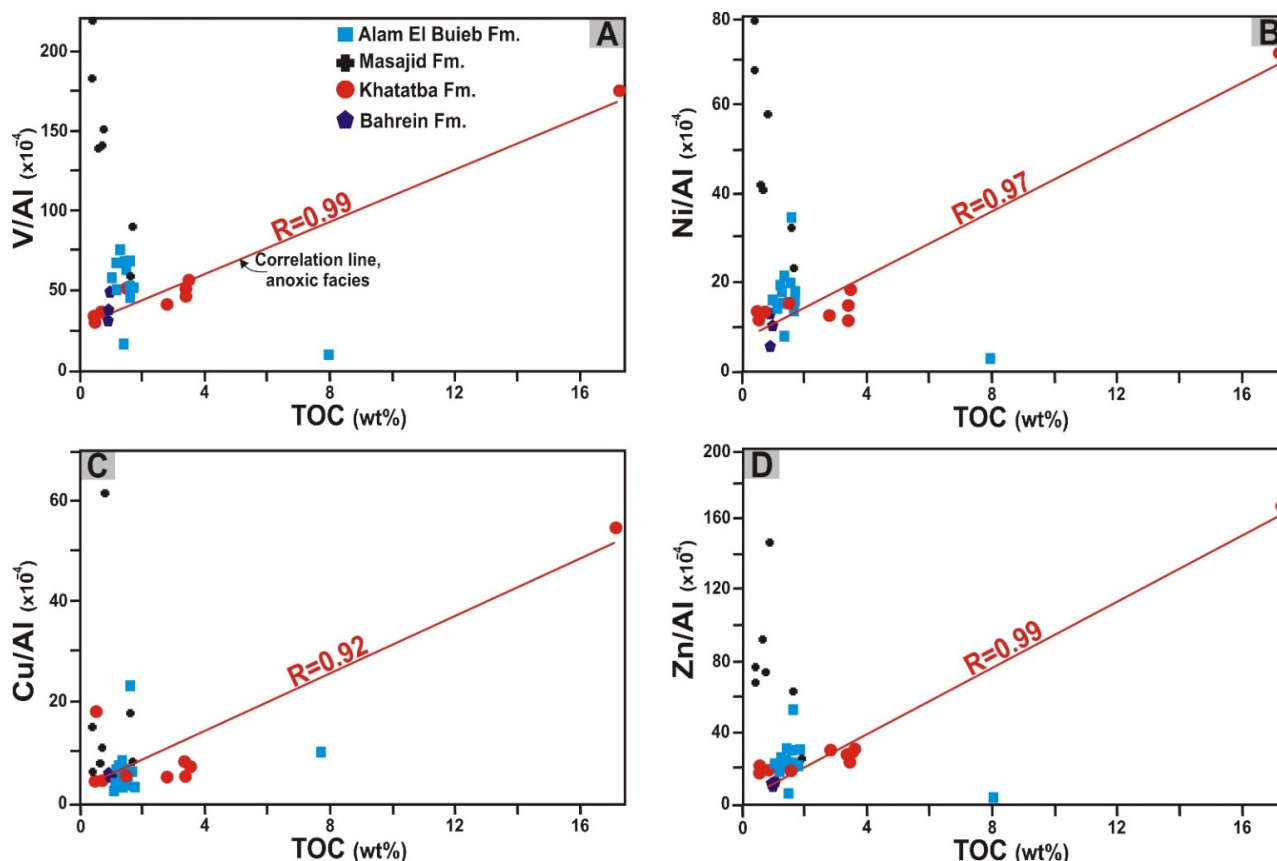


**Figure 4.** (A–D) Relationships between Al-normalized redox-sensitive elements of V, Ni, Cu, and Zn, respectively, versus TOC concentration for the Jurassic–Lower Cretaceous Bahrein, Khatatba, Masajid, and Alam El Bueib Formations in the Almaz-1 well, Shushan Basin (modified after Algeco and Maynard [28]). Lines of correlation in (A–D) are observed for Khatatba Formation samples.

#### 4.5. Detrital Influx and Weathering Proxies

To track the role of detrital/siliciclastic sediment flux, the elemental ratios of Si/Al versus K/Al (Figure 6), Ti/Al, Zr/Al, and (Zr + Rb)/Sr are reported. These ratios exhibit significantly similar trends, all of which are opposite to the carbonate profile (Figure 7, Supplementary Materials Table S1). Within the Bahrein and Khatatba formations, the Si/Al, Ti/Al, and Zr/Al ratios gradually increase to values in the range of 1.4–4.3 (2.8 on average), 0.07–0.18 (0.13 on average), and 17.3–101.7 (64.1 on average), respectively. This is consistent with the highest values in the (Zr + Rb)/Sr ratio throughout the studied succession that reach up to 5.3 (2.4 on average). This is followed by a significant decline in Ti/Al (0.18 to 0.004), Zr/Al (101.7 to 24.5), (Zr + Rb)/Sr (2 to 0.06), and, to some extent, the Si/Al ratio (2.6 to 0.8) from the uppermost Khatatba to Masajid Formations, respectively. In the lower part of the Alam El Bueib Formation, the Si/Al (0.6–7.8), Zr/Al (6.5–202), and Ti/Al ratios (0.02–0.2) display sharp peaks that represent the highest values throughout the

studied succession. The  $(Zr + Rb)/Sr$  ratio shows a significant increase from 0.2 to 3.1 that is consistent with remarkable peaks in the  $Zr/Al$ ,  $Ti/Al$ , and  $Si/Al$  ratios (Figure 7).

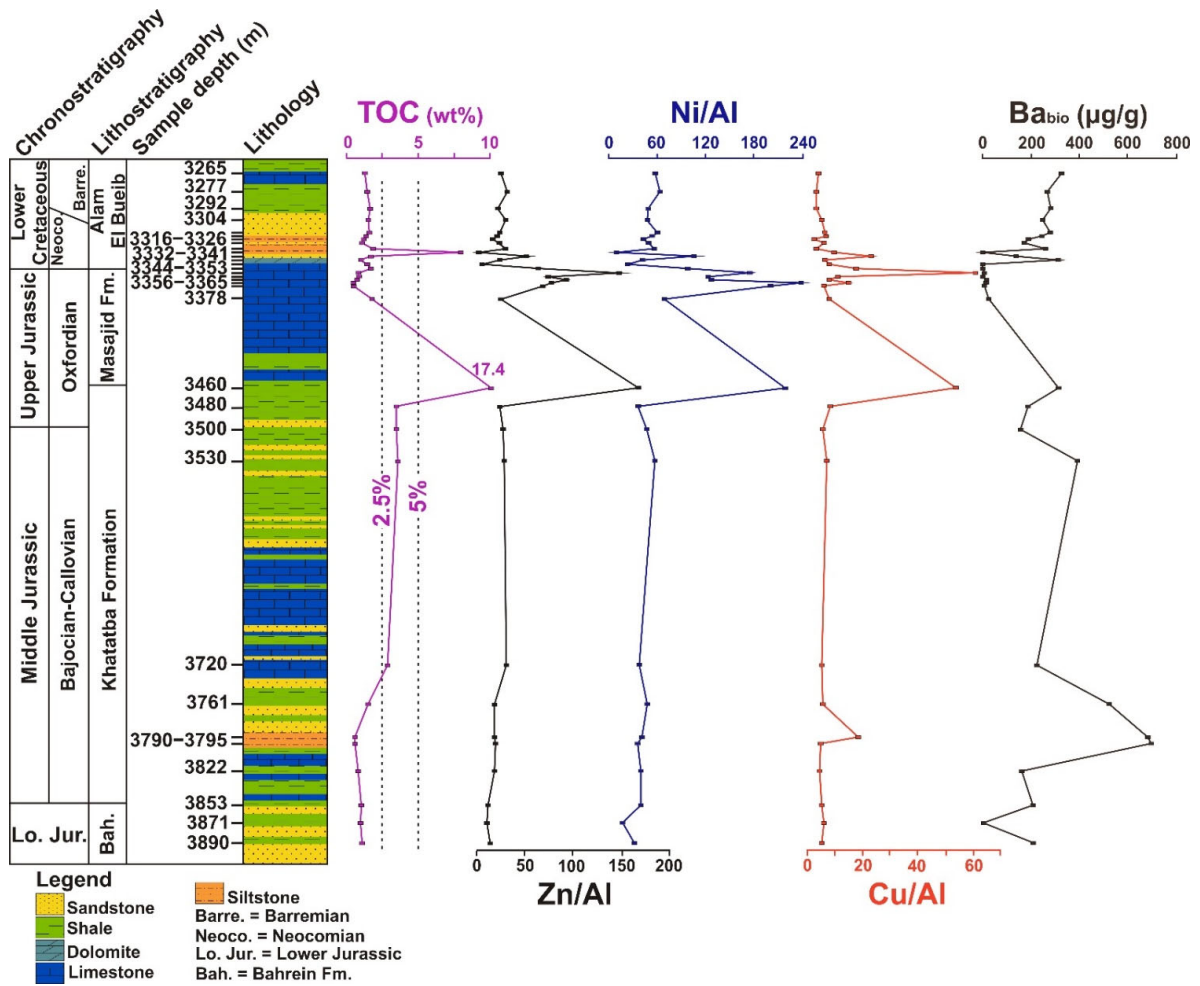


Figure 5. Chemostratigraphic distribution of TOC and paleoproductivity elemental proxies of the Jurassic–Lower Cretaceous sediments from the Almaz-1 well, Shushan Basin.

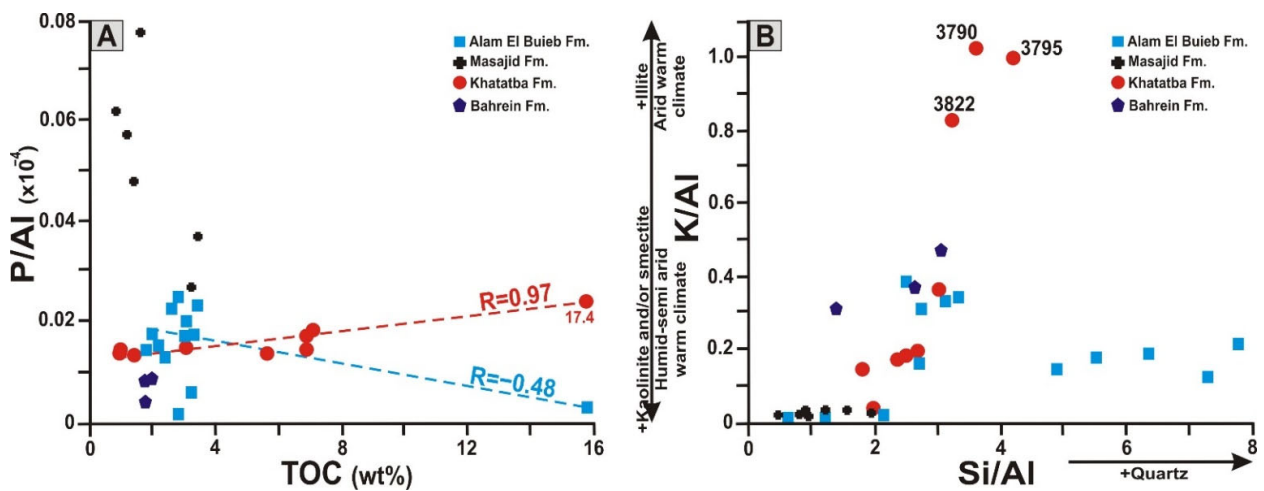
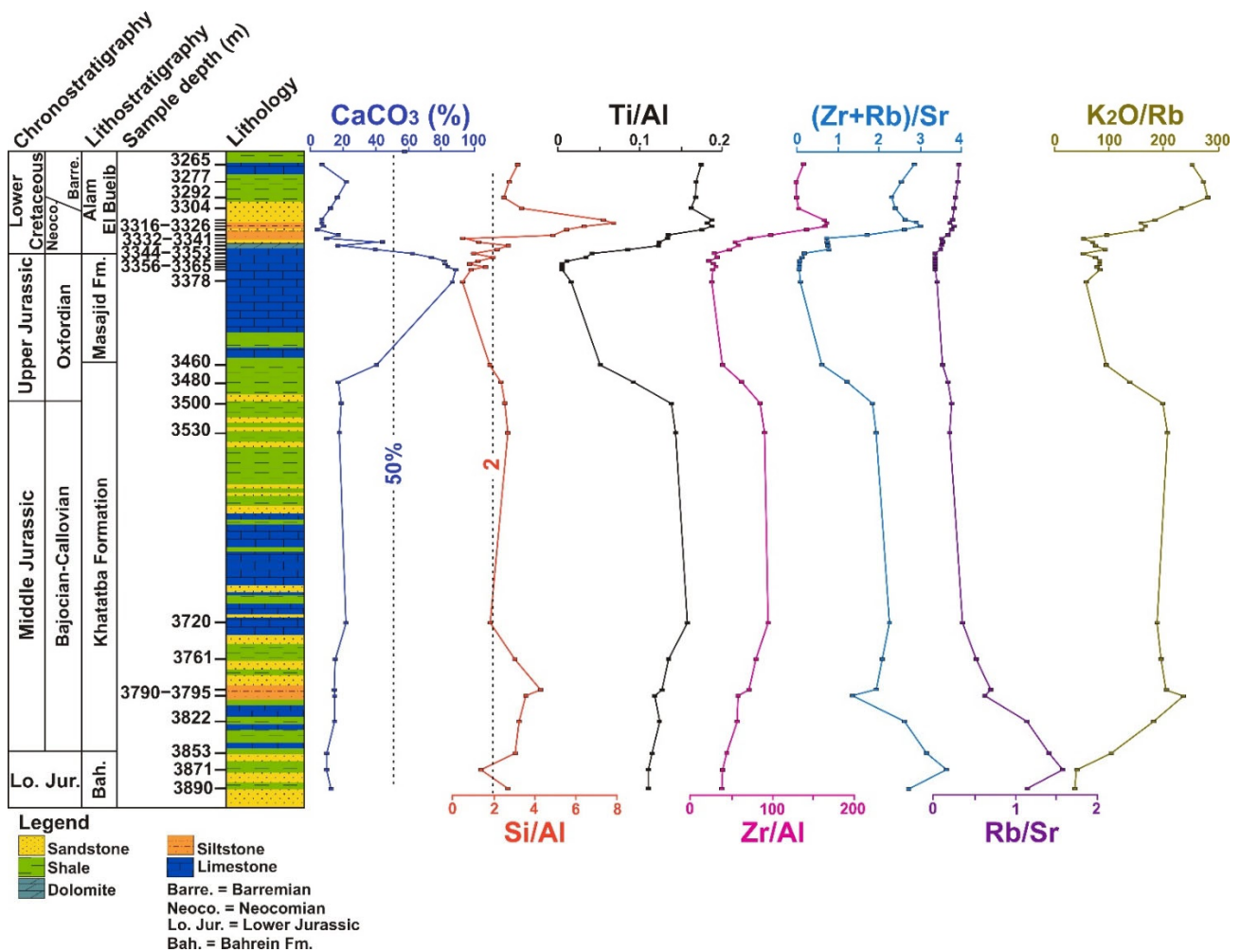


Figure 6. (A) Plot of the  $P/Al$  ratio versus TOC content. (B) Plot of  $K/Al$  against  $Si/Al$  ratios.



**Figure 7.** Chemostratigraphic distribution of carbonate content and geochemical elemental ratios employed to assess changes in abundance of terrigenous sediment supply and role of continental weathering during deposition of the Bahrein, Khatatba, Masajid, and Alam El Bueib Formations in the Almaz-1 well, Shushan Basin. Ratios of Ti/Al, Zr/Al, (Zr + Rb)/Sr, Rb/Sr, and K<sub>2</sub>O/Rb were smoothed with a 3-point moving average.

The K<sub>2</sub>O/Rb and Rb/Sr ratios exhibit opposite trends across the Bahrein Formation. Within the Khatatba and Masajid Formations, the Rb/Sr ratio shows a slight long-term decrease from 0.74 to 0.007, while the K<sub>2</sub>O/Rb displays a significant long-term decrease to minimum values from 247 to 16. The Rb/Sr ratio shows a minor increase in the range of 0.02–0.28 within the Alam El Bueib Formation, while the K<sub>2</sub>O/Rb drastically increases up to maximum values (from 16 to 311.3) throughout the studied succession (Figure 7).

## 5. Discussion

### 5.1. Redox Conditions and Paleoproductivity Assessment

Specific trace elements can be used as reliable proxies for redox conditions’ assessment due to their geochemical behavior and low solubility under oxygen-depleted environments [24]. Under reducing conditions, active abiotic processes trigger enhanced adsorption of metallic ions into organic matter or incorporation into sediments through mineral substrates as well as the precipitation of sulfide compounds and formation of organometallic complexes [29]. Specific trace elements, such as Mo, V, and U, and to some extent Cr and Co, tend to be less soluble and are more efficiently transferred from the water column to sediments under extensive anoxia [24], resulting in their authigenic enrichment

in sediments. Other redox-sensitive trace elements, including Ni, Cu, and Zn are delivered to sediments in combination with organic matter during periods of enhanced biological productivity [24] or they may be retained in sediments in association with pyrite after organic matter decay by sulfate-reducing bacteria [10,12,30]. Significant concentrations of organic matter within the sedimentary record can result from enhanced biological productivity in the water column of marine ecosystems. Assessment of marine primary productivity is conducted for the current study succession based on ratios of Ni, Cu, Zn, Ba, and P normalized to Al and their relationship with TOC concentration.

The Bahrein Formation is dominated by TOC-lean sediments that exhibit low  $V_{EF}$ ,  $Ni_{EF}$ ,  $Cu_{EF}$ ,  $Zn_{EF}$ , and  $Cr_{EF}$  (Figure 3). This indicates that the water column was well-oxygenated during deposition of this interval, which is not favorable for labile organic matter preservation [10]. This is consistent with the lack of correlation between Ni/Al ( $r = 0.13$ ), Cr/Al ( $r = 0.20$ ), and Cu/Al ratios ( $r = -0.76$ ) versus TOC content (Figure 4), suggesting that these redox-sensitive elements are decoupled from TOC flux during deposition. The  $V/(V + Ni)$  and  $V/Cr$  ratios can be used as proxies for paleoenvironmental conditions because these ratios remain unaltered during diagenesis possibly due to strong atomic bonds with high molecular-weight organics [31]. Thus, high  $V/(V + Ni)$  and  $V/Cr$  ratios are associated with severe anoxic conditions [32–34]. Applying the common thresholds of trace elements for the ratios  $V/(V + Ni)$  and  $V/Cr$  (Supplementary Materials Table S2), more overall reducing conditions are indicated than enrichment factors for these elements. For this interval, strong linear correlations between the former elements and Al content are observed (Cu:  $r = 0.93$ ; Zn:  $r = 0.89$ ; V:  $r = 0.80$ ; and Cr:  $r = 0.78$ , not shown), indicating that the concentration of these elements was controlled by lithological composition such as enhanced terrigenous sediment supply during deposition. Therefore, the source of these redox-sensitive elements is allochthonous (i.e., terrigenous) rather than being controlled mainly by authigenic enrichment under oxygen-depleted conditions [28]. Additionally, relatively low Zn/Al, Ni/Al, and Cu/Al values as well as the absence of correlation between the former ratios and TOC content reveal weak marine primary productivity during the time of the deposition of the Bahrein Formation.

Phosphorous is an important element in marine ecosystems and it contributes to many metabolic processes. Under dysoxic–anoxic bottom water conditions, phosphorous remobilizes and diffuses from the uppermost sediments at the substrate into the water column [35,36]. In this context, the significant increase in P regeneration into the overlying sediments may amplify phosphate recycling and, thus, a low burial efficiency of P that leads to increased water column primary productivity as a positive feedback mechanism [35]. Therefore, the relationship between P/Al and TOC content can be used as a proxy to indicate the role of marine primary productivity during deposition (Figure 6A). For the Bahrein Formation, P/Al displays a moderate covariation with the TOC content ( $r = 0.52$ ), indicating that enhanced P concentration was controlled by several sources, either by enhanced terrigenous supply of detrital P or partially related to organic carbon supply as authigenic P during deposition under low primary productivity.

Barium concentration in sediments can be used to assess the role of marine primary productivity [37]. It is present in the water column and accumulates in the sediment in the form of barite, which is formed during organic matter destruction and decomposition under oxic conditions [38] or phases of early diagenesis [39]. Barite may also be remobilized, which leads to Ba release during phases of phytoplanktonic decay [40]. This would trigger a part of the enhancing of water column biological productivity. For the Bahrein Formation, the  $Ba_{bio}$  is low (0 to 212 ppm, 139 ppm on average), indicating deposition of these sediments under low productivity conditions [26,27].

The Middle Jurassic Khatatba Formation is characterized by the highest TOC content, especially in the middle and upper parts (Figure 3). It is dominated by low to moderate enrichment of  $V_{EF}$ ,  $Ni_{EF}$ ,  $Zn_{EF}$ ,  $Cu_{EF}$ , and  $Cr_{EF}$ , except for the sample at a depth of 3460 m that shows significantly high enrichment of these redox-sensitive elements (Figure 3). Excess enrichment of these redox-sensitive elements indicates that deposition took place

under enhanced oxygen-deficient conditions in the water column and at the sediment–water interface [13]. This is consistent with high values of the  $V/(V + Ni)$  ratio that fall within the common thresholds of enhanced water column anoxic conditions (Table S2) [31,32,34]. However, the  $V/Cr$  ratios suggest slightly lower oxygen-depleted water column conditions (dysoxic to oxic) during deposition of the Khatatba Formation that are not consistent with enrichment factors of redox-sensitive metals and the  $V/(V + Ni)$  ratios. Ratios of  $V/Al$ ,  $Ni/Al$ ,  $Cu/Al$ ,  $Zn/Al$ , and  $Cr/Al$  show strong linear correlations with the TOC content (Figure 4B–D), suggesting that deposition of the Khatatba Formation was controlled by enhanced organic matter supply into sediments under prevalent basin anoxia [24,28]. This interpretation is supported by the lack of correlation between redox-sensitive metals and Al concentration ( $Cu: r = 0.02$ ;  $Zn: r = 0.03$ ;  $V: r = -0.07$ ;  $Cr: r = 0.19$ ;  $Ni: r = 0.14$ ), reinforcing their authigenic enrichment and, thus, they are associated with anoxic conditions [24,28]. Recent investigations of the Khatatba Formation from the adjoining Falak-21 well in the Shushan Basin indicated that abundant total sulfur content is consistent with the occurrence of pyrite due to available reactive Fe in the water column and deposition under enhanced anoxic conditions at the sediment–water interface [5]. Additionally, anoxic conditions during deposition of the Khatatba Formation are suggested to be controlled primarily by changes in the paleogeographic conditions and oscillations between the low relief swamp belt in the north Western Desert and the marine inundation of the Tethys toward the south that led to a stagnant water column and the accumulation of organic carbon-rich intervals [41]. Furthermore, previous palynological and palynofacies studies indicated that the middle interval of the Khatatba Formation was deposited in deltaic to shallow marine, oxygen-depleted conditions, whereas the upper interval was deposited under fluvio-deltaic to restricted shallow restricted marine conditions [5,42]. The strong relationships of the former ratios of Al-normalized Ni, Cu, and Zn with TOC content indicate that the coupling of these elements' enrichment with the available organic matter in the Khatatba sediments refers to their behavior as micro-nutrients [24,28]. Therefore, deposition of the Khatatba Formation took place under enhanced marine paleoproductivity and organic carbon export via enhanced organic matter production and preservation in the sediments in deficient oxygenation conditions [10,12]. This is consistent with the highest Ba concentration within the Khatatba Formation relative to the studied succession that reaches maximum values of 862 ppm, which are greater than the average Upper Continental Crust (UCC: 668 ppm [25]). Additionally, the  $Ba_{bio}$  exhibits a major peak with a long-term rise to maximum values of 709 ppm, which is consistent with the onset of increased organic carbon accumulation in the Khatatba Formation. The  $P/Al$  ratio shows a strong linear correlation with the TOC content ( $r = 0.98$ ) along with a significant concentration of  $Ba_{bio}$ , suggesting high marine primary productivity and organic carbon supply into the sediments at the time of deposition of the Khatatba Formation. This is in agreement with previous studies that interpreted the Khatatba Formation as an excellent source rock with high organic matter enrichment and hydrocarbon generation potential throughout the north Western Desert [5–7]. In the event of prevalent anoxia in the bottom water environment, as is the case of the Khatatba Formation, regenerated P can be sequestered through adsorption and/or co-precipitation into authigenic P-bearing minerals (e.g., authigenic apatite). Similar observations were reported from the Toarcian oceanic anoxic event Quse oil shales, Tibet [43], as well as the Cenomanian–Turonian anoxic event [36]. As a consequence, the enrichment of benthic microbial mats in the uppermost sediments and at the sediment–water interface can result in the limited exchange of remobilized P between the sediment pore space and bottom water [24], which would promote quantitative sequestration of remobilized P within sediments during anoxic conditions.

The Upper Jurassic Masajid carbonates are dominated by low to moderate concentration of the TOC content (0.9 wt% on average) versus high enrichment of redox-sensitive trace elements (Figure 3). However, the enrichment of  $V_{EF}$ ,  $Ni_{EF}$ ,  $Zn_{EF}$ ,  $Cu_{EF}$ , and  $Cr_{EF}$  within the Masajid Formation is interpreted to be controlled by enhanced carbonate production in the water column due to depleted organic matter content and terrigenous sediment

supply (i.e., a minimum contribution of Al and Si). Our hypothesis is supported by moderate correlations between V/Al ( $r = 0.56$ ), Cr/Al ( $r = 0.55$ ), and Ni/Al ( $r = 0.26$ ) versus the carbonate content. In contrast, the lack of a correlation between Cu/Al ( $r = -0.04$ ) versus TOC and moderate to strong negative correlations between Zn/Al ( $r = -0.50$ ), Cr/Al ( $r = -0.82$ ), V/Al ( $r = -0.81$ ), and Ni/Al ratios ( $r = -0.74$ ) versus TOC content (Figure 4), suggests that these elements are decoupled from organic carbon supply, and deposition of this interval took place under low marine primary productivity and prevalent oxic–dysoxic conditions [28]. Therefore, relatively high  $V_{EF}$ ,  $Ni_{EF}$ ,  $Zn_{EF}$ ,  $Cu_{EF}$ , and  $Cr_{EF}$  cannot be interpreted as being triggered by authigenic enrichment under enhanced bottom water anoxia, and, instead, their excess enrichment is attributed to lithological properties [43]. The V/Cr ratios show a long-term decrease in minimum values in the Masajid Formation (Figure 3), which suggests enhanced oxic conditions [33,34]. Although the V/(V + Ni) ratio exhibits similar trends to the V/Cr ratio, the values indicate deposition during severe oxygen-depleted conditions, which contradicts the previous results. The  $Ba_{bio}$  concentrations are significantly low within the Masajid Formation, which shows a weak correlation with the TOC content ( $r = 0.33$ ). This indicates that Ba concentration is decoupled from organic matter supply and deposition of the Masajid Formation under low marine primary productivity conditions. Similarly, the P/Al ratio exhibits a strong negative correlation with the TOC ( $r = -0.79$ ) (Figure 6A), reinforcing a weak marine productivity of organic matter during deposition.

The Lower Cretaceous Alam El Bueib Formation is characterized by low average values of TOC content and a limited degree of authigenic enrichment of  $Ni_{EF}$ ,  $Zn_{EF}$ ,  $Cu_{EF}$ , and  $Cr_{EF}$  compared to  $V_{EF}$  that shows a moderate enrichment (Figure 3). This is consistent with the moderate negative correlations between V/Al ( $r = -0.65$ ), Cr/Al ( $r = -0.57$ ), Ni/Al ( $r = -0.52$ ), and Zn/Al ( $r = -0.47$ ) versus TOC content, whereas Cu/Al ( $r = 0.20$ ) shows a weak correlation with TOC content (Figure 4). The lack of correlation between the TOC content and the former redox-sensitive elemental ratios suggests deposition under enhanced oxic to dysoxic conditions of the water column [24,28]. The moderate and strong correlation between Cr ( $r = 0.48$ ) and Cu ( $r = 0.97$ ) versus Al content suggests that both elements were derived from enhanced terrigenous clastic supply during deposition. The V/Cr ratio shows a long-term increase in average values from 1.7 to 2.2 across the Alam El Bueib Formation (Figure 3), which suggests deposition under prevalent oxic to dysoxic conditions [33,34]. The V/(V + Ni) ratio displays a similar trend to the V/Cr ratio, but it infers more reducing conditions overall that are not consistent with the V/Cr ratios and co-variation between the TOC and redox-sensitive metals. The productivity proxies of Zn/Al, Ni/Al, and Cu/Al exhibit a long-term fall within the Alam El Bueib Formation compared to the underlying Masajid carbonates. Additionally, the moderate correlations between carbonate content and Cu/Al ( $r = 0.61$ ), Ni/Al ( $r = 0.32$ ), and Zn/Al ( $r = 0.29$ ), and the absence of a correlation between these ratios and the TOC content, supports the hypothesis that their availability is partially related to enhanced carbonate production and the limited diffusion of organic matter supply during low marine primary productivity. Our results are similar to the organic matter characterization of the Alam El Bueib Formation from the adjoining Shams gas field in the Shushan Basin [8], whereby this interval was dominated by poor to fair organic carbon-richness due to the relatively low marine productivity during deposition. Despite the  $Ba_{bio}$  showing a long-term rise interrupted by minor falls, the  $Ba_{bio}$  values are slightly higher (up to 319 ppm, 206 ppm on average, Figure 5) than the common threshold of average values of low marine productivity (<200 ppm) [26,27,44]. Additionally, a negative correlation is observed between the P/Al ratio and the TOC content for the Alam El Bueib Formation ( $r = -0.48$ ), indicating low marine primary productivity due to the lack of P regeneration and sequestration into authigenic P-bearing minerals in response to enhanced water column oxic respiration [35,36].

## 5.2. Characterization of Detrital Sediment Flux

Variations in the chemical composition of sediment fractions show evidence of periodic fluctuations in the abundance of terrigenous sediment input, as reflected in the accumulated siliciclastic- and carbonate mineral-associated elements (Figure 7). This can be inferred from siliciclastic mineral-associated elements, such as Si, Zr, Ti, and their ratios normalized to Al. For example, the relative abundance of Si, and thus Si/Al, in a predominantly detrital interval can be used as a reliable proxy for relative changes in the proportions of silt to clay fractions [45]. Titanium (Ti) is enriched in heavy minerals, such as ilmenite and rutile, which settle out sooner compared to Al-bearing clay mineral fractions [46]. Thus, the Ti/Al ratio can be used to reflect inferences about changes in proximity to detrital source terranes and terrigenous sediments input to the basin [47]. Similarly, Zirconium (Zr) is present in heavy mineral fractions of silt-size detrital zircon, and, thus, the Zr/Al ratio can reveal changes in terrigenous coarse sediment supply [43,48,49]. Rubidium (Rb), in contrast to Zr, is enriched in clay mineral fractions, mostly in illite [50], whereas Sr is confined in carbonate minerals [51]. These properties make it possible to implement the (Zr + Rb)/Sr ratio as an indicator for variations in siliciclastic sediment supply relative to carbonates in sedimentary successions [52].

The Bahrein Formation and the lower–middle parts of the Khatatba Formation are characterized by slightly lower average values of Si/Al ratios (2.7 on average) than the UCC (4.33) and the post-Archaean Australian shale (PAAS, 3.32; [46]). This interval shows a slight long-term rise in Si/Al, Ti/Al, and Zr/Al. The increase in these ratios can be attributed to a gradual coarsening in the grain size of fine clastic sediments during deposition, such as a change from shale to coarse silt- and sand-size fractions [48,49]. The Si/Al shows a gradual fall at depths of 3761 m and 3720 m that is possibly related to a vertical change in facies from fine-sized clays to carbonate-precipitated minerals during low coarse clastic supply to the basin (Figure 7). However, the Bahrein Formation and the lower part of the Khatatba Formation show a slightly opposite trend in (Zr + Rb)/Sr to the Si/Al, Zr/Al and Ti/Al ratios (Figure 7). Rising (Zr + Rb)/Sr values are indicative of an increase in siliciclastic-dominated facies compared to limited carbonate deposition. From the upper part of the Khatatba to the upper Masajid formations, all detrital proxies (i.e., Si/Al, Ti/Al, Zr/Al, and (Zr + Rb)/Sr) show a strong long-term decline toward minimum values (Figure 7). This can be interpreted in terms of limited terrigenous supply during enhanced carbonate deposition of the Masajid Formation at times of a Late Jurassic major marine transgression in northern Egypt [17,53]. This is consistent with strong negative correlations between Ti/Al ( $r = -0.94$ ,  $p < 0.01$ ,  $n = 7$ ), (Zr + Rb)/Sr ( $r = -0.83$ ,  $p = 0.02$ ,  $n = 7$ ), and Zr/Al ( $r = -0.70$ ,  $p = 0.08$ ,  $n = 7$ ) and carbonate content in the Masajid Formation.

Pronounced differences observed between the former geochemical proxies and carbonate content (Figure 7) confirm that the studied succession consists mainly of considerable proportions of fine silts and clays versus carbonates. This can be delineated from the SiO<sub>2</sub>–Al<sub>2</sub>O<sub>3</sub>–CaO ternary plot (Figure 8). This ternary diagram illustrates that samples of the Bahrein and Khatatba Formations plot toward the line of average shale [25]. Only the sample at a depth of 3871 m from the Bahrein Formation plots at the zone of excess clay mineral fractions, whereas the sample depth 3460 m in the Khatatba Formation plots in the zone of increased carbonate content (Figure 8). In contrast, all samples of the Masajid Formation plot in the zone of highest carbonate content (Figure 8), in agreement with the lowest contribution of terrigenous coarse clastic sediment supply as evidenced by the Si/Al, Ti/Al, Zr/Al, and (Zr + Rb)/Sr ratios.

Within the Alam El Bueib Formation, a significant increase with remarkable peaks in the Si/Al, Ti/Al, Zr/Al, and (Zr + Rb)/Sr ratios are reported, which are consistent with minimum values in carbonate content (Figure 7). These rising ratios can be interpreted to infer increased proportions of sand- and coarse silt-size detrital mineral fractions compared to clay and carbonate minerals [43,45,48,52] during a phase of enhanced terrigenous sediment supply and proximity to the coastline at times of a sea level fall. This is in agreement with the plot of these samples in the SiO<sub>2</sub>–Al<sub>2</sub>O<sub>3</sub>–CaO ternary plot toward the zone of

enhanced quartz contribution (Figure 8). This is followed by a minor fall in the Si/Al, Ti/Al, Zr/Al, and (Zr + Rb)/Sr ratios (Figure 7) that is related to a decrease in the coarse silt-size fraction and enhanced accumulation of the clay-size fraction as evidenced by a thick interval of shale interrupted by a thin limestone unit. This is consistent with the plot of samples of this interval along the line of average shale (Figure 8).

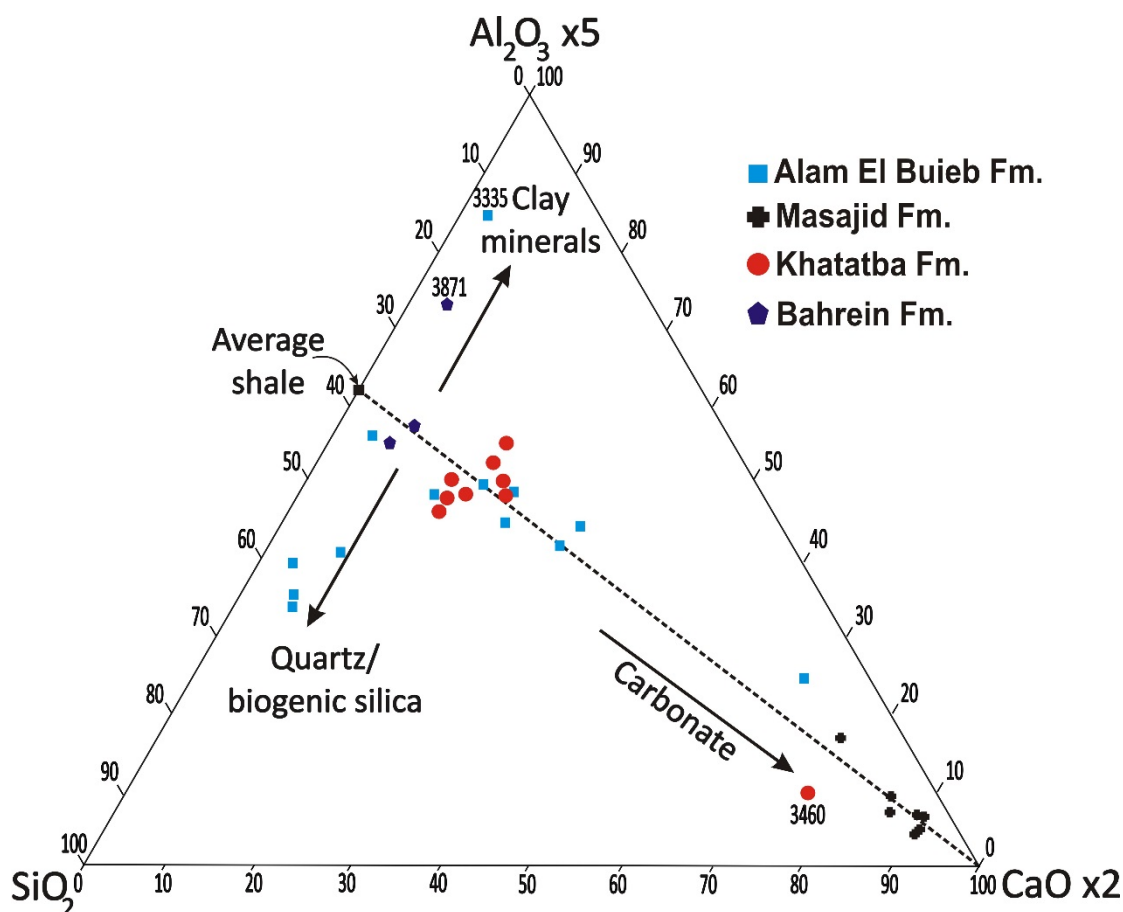


**Figure 8.** Geochemical ternary plot of  $\text{SiO}_2-5*\text{Al}_2\text{O}_3-2*\text{CaO}$  to reveal variations in lithological differences of the Jurassic–Lower Cretaceous sediments in the Almaz-1 well. Most samples scatter around the line of average shales and carbonates [25]. Four samples from the Alam El Bueib Formation showed enhanced contribution of quartz, while two samples from the Bahrein and Alam El Bueib formations were dominated by clay minerals.

### 5.3. Paleoclimatic Conditions and Continental Weathering

Rb/Sr and  $\text{K}_2\text{O}/\text{Rb}$  ratios can be used as reliable proxy indicators to assess changes in the continental weathering at the source terrane and related siliciclastic sediment supply [54]. They can also be used along with the K/Al versus Si/Al ratios to trace the paleoclimatic variations during deposition [12,43,45,48,55]. Higher values in Rb/Sr would indicate periods of active continental weathering and terrestrial riverine runoff compared to  $\text{K}_2\text{O}/\text{Rb}$ , which tends to decrease. This is because  $\text{Rb}^+$ , which is a large alkali trace metal, is retained more at sites of the exchange of clays compared to the smaller  $\text{Sr}^{2+}$  [54]. During active weathering conditions, the average values of the  $\text{K}_2\text{O}/\text{Rb}$  ratio tend to decrease relative to the average values of the UCC that reach a value of 252 [46,54]. In contrast, the Rb/Sr values drastically increase ( $>1$ ) during phases of strong continental weathering conditions relative to the average values of the UCC (0.32 [54]). Recently, the weathering intensity was defined as the ratio between the rates of chemical silicate weathering and the total denudation rates [55,56]. For this purpose, specific proxies such as Li and Si isotopes

and their relationships with Li/Na and Li/Mg are implemented [55,56]. The K/Al ratio is commonly used to infer clay mineral composition in sediments, whereby low ratios indicate the enhanced concentration of kaolinite/smectite and deposition of sediments under a prevalent humid to semi-arid warm climate compared to high ratios that imply the enhanced contribution of a micaceous clay/illite composition and accumulation of sediments under an arid warm climate [12,43,48,57].

The elemental ratios of Rb/Sr and K<sub>2</sub>O/Rb exhibit significantly opposite trends across the Bahrein Formation and the lower part of the Khatatba Formations (Figure 7). The K<sub>2</sub>O/Rb shows a sudden rise from 166 to 247, which is similar to the value of the UCC as opposed to a sharp decline in the Rb/Sr (from 2.6 to 5.3, 2.5 on average), suggesting active hydrological cycle and continental weathering triggered by prevalent greenhouse conditions [43]. This interpretation is supported by the significant rise in the Si/Al and (Zr + Rb)/Sr ratios as well as a strong negative correlation between Rb/Sr and carbonate content ( $r = -0.93$ ), revealing an active terrigenous supply compared to depleted carbonate production in the water column [52,54]. It was indicated that Rb/Sr ratios are a sensitive elemental proxy for climatic changes with ratios higher than 0.03 revealing a warm humid climate [58]. The Bahrein Formation is characterized by significantly high Rb/Sr with average values of 1.6, indicating prevalent warm and humid climate conditions at this time. Additionally, the plot of the K/Al against Si/Al shows strong linear relationship for the Bahrein Formation ( $r = 0.91$ ), which indicates the enhanced contribution of kaolinite and/or smectite, and to a lesser extent illite, and deposition under prevalent warm humid to semi-arid climates [12,43,57]. This is consistent with climatic interpretations based on recovered dinoflagellate cysts from the East Faghour-1 well that is located to the west of the Shushan Basin, which revealed deposition of the Bahrein Formation at times of enhanced humid tropical to subtropical paleoclimatic conditions [42].

Within the middle to upper parts of the Khatatba Formation and the carbonate-rich Masajid Formation, the Rb/Sr ratio gradually decreases to minimum values from 0.73 to 0.008 (0.12 on average), which is consistent with a sharp decline in K<sub>2</sub>O/Rb from 247 to 60 (79 on average). These values are significantly lower than the average values of the UCC, indicating weak continental weathering and terrestrial discharge during the deposition of these sediments. This is consistent with strong negative correlations between Rb/Sr ( $r = -0.75$ ) and K<sub>2</sub>O/Rb ( $r = -0.73$ ) versus carbonate content that is significantly increased to maxima (up to 89.2%, Figure 7). Despite the Rb/Sr ratio showing a long-term fall within the Khatatba Formation, it exceeds the average values of 0.03 compared to the Masajid Formation that contains the lowest Rb/Sr values (0.01 on average) [58], indicating deposition of both formations under warm humid to arid climates, respectively. The K/Al ratio exhibits a strong covariation with the Si/Al ratio ( $r = 0.92$ ), whereby the lowest three samples are characterized by significant illite compared to the middle and upper parts of the Khatatba Formation that show an increase in kaolinite and smectite (Figure 6B). This indicates deposition of the Khatatba Formation under semi-arid to warm humid climates [12,43,57]. This is supported by assessed climatic conditions according to recovered dinoflagellate cysts, spores, and pollen grains from the East Faghour-1 well [42], which indicated deposition of the Khatatba Formation under mainly warm humid climates. Further palynological work from the Shushan Basin indicated that the Upper Jurassic Masajid Formation was deposited at times of warm semi-arid to arid climates in adjacent hinterlands with local wetland vegetation based on the common occurrences of the gymnosperm pollen grains *Classopollis*, *Spheripollenites*, and *Araucariacites* [59]. This is in agreement with the lowest values of the K/Al and Si/Al ratios in the Masajid Formation, suggesting a minor contribution of clay minerals and reinforcing deposition under warm semi-humid to semi-arid climates [12,43,57].

The Alam Al Bueib Formation is characterized by a minor long-term increase in the Rb/Sr ratio up to 0.35 (0.19 on average) [54]. The K<sub>2</sub>O/Rb ratio through the Alam Al Bueib Formation shows a vertical change in values from a minimum (10 on average) to a maximum of 311 (160 on average). The values of both ratios suggest variable degrees

of continental weathering. The  $K_2O/Rb$  values that are below 252 in sandstone and siltstone facies of the lower part of the Alam Al Bueib Formation suggest strong continental weathering, which are in agreement with major peaks in proxies of terrigenous clastic supply, including  $Si/Al$ ,  $Ti/Al$ ,  $Zr/Al$ , and  $(Zr + Rb)/Sr$ . The significantly high  $K_2O/Rb$  values recorded within the upper shale and limestone interval of the Alam Al Bueib Formation indicate moderate to weak continental weathering, which is consistent with the lower contribution of terrigenous coarse clastic supply [46] (Figure 7). This is supported by strong and moderate positive correlations between the  $K_2O/Rb$  ratio and  $(Zr + Rb)/Sr$  ( $r = 0.76$ ) and  $Zr/Al$  ( $r = 0.56$ ). The slight long-term rise in the  $Rb/Sr$  within the Alam Al Bueib Formation exceeds average values of 0.03 [58], indicating deposition during a warm humid climate. The plot of the  $K/Al$  versus  $Si/Al$  ratios shows no correlations for the Alam Al Bueib samples, which are randomly distributed between low to moderate values of  $K/Al$  with no clear pattern (Figure 6B). Relatively low  $K/Al$  ratios indicate the enhanced contribution of kaolinite and/or smectite in clay-rich intervals and deposition under warm humid to semi-arid climates compared to intervals with slightly higher  $K/Al$  ratios that would include some illite, and, thus, deposition under a warm arid climate (Figure 6B) [12,43,57].

#### 5.4. Major Controlling Processes of Organic Carbon Accumulation

Organic carbon accumulation is one of the most important factors for hydrocarbon source rock enrichment and generating potential. The primary drivers that control organic carbon accumulation have been commonly investigated. This includes sedimentological processes of the three endmembers of carbonate, siliciclastic, and organic carbon flux [60], Rock-Eval measured parameters versus bioturbation processes [61], sulfide formation and available iron content [62], elemental geochemistry and dinoflagellate cyst composition [12], and sedimentation rates versus level of oxygenation conditions [13]. The current study succession contains varied proportions of organic carbon in fine clastic shales and siltstones of the Khatatba and Alam El Bueib Formations versus carbonates of the Masajid Formation; thus, a discussion of primary environmental drivers by which organic matter accumulates is required. In this context, organic matter accumulation in sediments is largely controlled by several factors, such as the sedimentation rate, role of redox conditions, accommodation space or relative sea level, marine primary productivity and terrestrial input, or the type of water column conditions [10–13].

The Middle Jurassic Khatatba Formation is characterized by moderate to high enrichment of organic carbon and low to moderate carbonate content (Figure 3). During deposition, high marine primary productivity and enhanced riverine runoff in the Shushan Basin likely induced enhanced water column stratification conditions (Figure 9A). At this time, active spreading and rifting in the north Western Desert [15,16] triggered some changes in the paleogeographic position during deposition in the study area, which resulted in a fluctuation between the low relief fluvial or swamp belt and the minor marine inundation of the Tethys Ocean toward the south [5,41,42]. This led to restricted oceanographic and circulation patterns that might occur at this time, and, thus, limited water mass exchange and stagnant water column conditions were prevalent during deposition. These conditions triggered moderate to high concentrations of redox-sensitive trace elements into the Shushan Basin (Figure 9A). Mansour et al. [5] indicated moderate to high total sulfur and TOC contents in sediments of the Khatatba Formation, whereby deposition of the Khatatba samples was controlled by reduced bottom water conditions, mainly suboxic to anoxic. Therefore, predominantly redox conditions and water column stratification during enhanced organic matter production triggered the enhanced preservation of organic carbon (Figure 9A). Additionally, an abundant contribution of clay mineral fractions (Figure 8), especially in the upper part of the Khatatba Formation as indicated by black shale deposition, provided favorable mineralogical conditions with an enhanced mineral surface area [63]. The availability of a large clay mineral surface area triggered, along with enhanced oxygen deficiency, carbon sequestration and the preservation of organic

carbon content [13]. Thus, the organic carbon-controlled processes during deposition of the Khatatba Formation enhanced the production and preservation versus limiting the dilution and decomposition of the available labile organic matter [11].

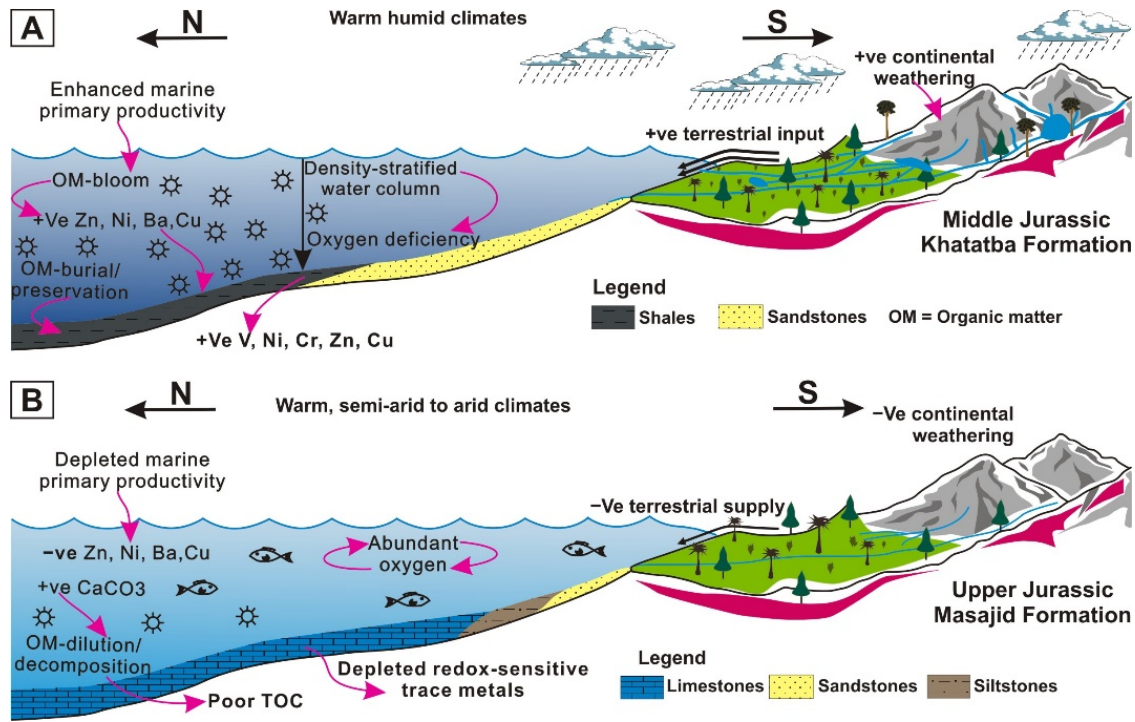


**Figure 9.** Paleoenvironmental processes prevalent during deposition of the Middle Jurassic Khatatba Formation (A) and the Upper Jurassic Masajid carbonates (B).

Different paleoenvironmental conditions and ecologic processes have been reported during deposition of the Masajid Formation that led to organic carbon-poor contents (Figure 9B). A moderate negative correlation ( $r = -0.43$ ) is observed between the TOC and carbonate contents. This indicates that the active carbonate dilution effect of labile organic matter controlled poor organic carbon preservation and burial in the sediments [11,13,60]. Additionally, organic carbon accumulation of the Masajid Formation was affected by oxic respiration versus low marine primary productivity conditions in the water column at times of deposition, which triggered the efficient decomposition and removal of labile organic matter (Figure 9B), especially if the sedimentation rate was low. This is because oxygen-respiring bacteria oxidize a high-proportion of the organic matter in enhanced ventilation environments and at low sedimentation rates, and, therefore, more organic carbon is decomposed [64].

The Alam El Bueib Formation contains low to moderate carbonate and TOC contents, except for the sample at a depth of 3335 m that contains high TOC content (Figure 3). The lithological composition of the studied interval of the Alam El Bueib Formation is characterized by alternations between sandstones, siltstones, and shales with minor carbonate interbeds (Figure 2). During deposition of these sedimentary facies, weak marine primary productivity dominated. Additionally, the enhanced supply of terrigenous coarse clastic sediments took place during deposition of the Alam El Bueib Formation. These environmental conditions resulted in the significant mineralization of labile organic matter through cyclic variations in siliciclastic input versus carbonate production, all of which triggered enhanced dilution and decomposition of the organic carbon supply [12,13,60]. Moreover, enhanced oxygenation conditions in the pore and bottom water that was prevalent during deposition were not favorable for the enhanced preservation and burial of organic matter.

## 6. Conclusions

The Jurassic–Early Cretaceous was a time of complex environmental processes in the Shushan Basin, north Western Desert, Egypt. Based on geochemical investigations of major and trace elements, carbonates, and TOC contents of the Bahrein, Khatatba, Masajid, and Alam El Bueib Formations, significant conclusions related to paleo-redox conditions, marine primary productivity, the role of sediment fluxes, and weathering intensity were developed. The Bahrein Formation is characterized by organic carbon-lean sediments deposited under oxic respiration and weak marine productivity conditions, along with enhanced terrigenous coarse clastic sediment supply due to active hydrological cycles and continental weathering rates under enhanced warm humid climates. The Khatatba Formation is one of the main hydrocarbon source rocks throughout the north Western Desert. It was deposited during enhanced marine productivity and organic carbon export under oxygen-depleted bottom water conditions, mainly suboxic to anoxic, under warm humid climate conditions. These conditions triggered the enhanced production and preservation of organic carbon versus the restricted dilution and decomposition of available labile organic matter. The lower part of the Khatatba Formation attested to predominant terrigenous sediment supply and active weathering conditions compared to the upper part that was deposited at times of limited terrigenous sediment supply due to weak continental weathering and enhanced carbonate production. The carbonate Masajid Formation was deposited under low marine primary productivity and prevalent oxic–dysoxic conditions, leading to the accumulation of organic carbon-poor sediments due to an enhanced carbonate dilution effect and the destruction of labile organic matter. The terrigenous sediment supply and continental weathering reached a minimum during deposition of the Masajid Formation compared to the enhanced carbonate production in response to a major marine transgression in northern Egypt and deposition under semi-arid to arid climates. The Alam El Bueib Formation attested to predominant ventilation in the pore and bottom water and the limited diffusion of labile organic matter due to low marine productivity, which were not favorable for the enhanced preservation of organic matter. The geochemical characterization of the Alam El Bueib Formation demonstrated active continental weathering and increased terrigenous proportions of sand- and coarse silt-size supply to the basin in the lower part and deposition under warm humid to semi-arid climates. In contrast, the upper part of Alam El Bueib was deposited under warm arid climates, moderate to weak continental weathering, and lower contribution of a terrigenous coarse clastic supply.

**Supplementary Materials:** The following supporting information can be downloaded at: <https://www.mdpi.com/article/10.3390/min12101213/s1>, Table S1: Measured values of major oxides and trace elements from the Jurassic–Lower Cretaceous Bahrein, Khatatba, Masajid, and Alam El Bueib formations in the Almaz-1 well, Shushan Basin, north Western Desert, Egypt. Table S2: Common thresholds used to interpret paleoredox conditions in this study.

**Author Contributions:** Conceptualization, A.M. and T.G.; methodology, A.M.; software, A.M.; validation, A.M., I.M.I. and M.S.A.; formal analysis, A.M.; investigation, A.M.; resources, M.W.; data curation, M.W.; writing—original draft preparation, A.M.; writing—review and editing, T.G.; visualization, M.W., I.M.I. and M.S.A.; supervision, T.G. and M.W.; project administration, A.M. and M.S.A.; funding acquisition, M.S.A. All authors have read and agreed to the published version of the manuscript.

**Funding:** This research was funded by Researchers Supporting project number (RSP2022R455), King Saud University, Riyadh, Saudi Arabia.

**Acknowledgments:** We are thankful to the Egyptian General Petroleum Corporation for their permission in providing cutting rock samples of the Almaz-1 well to conduct this study.

**Conflicts of Interest:** The authors declare no conflict of interest.

## References

1. Dromart, G.; Garcia, J.-P.; Picard, S.; Atrops, F.; Lécuyer, C.; Sheppard, S.M.F. Ice age at the Middle-Late Jurassic transition? *Earth Planet. Sci. Lett.* **2003**, *213*, 205–220. [[CrossRef](#)]
2. Jenkyns, H.C.; Schouten-Huibers, L.; Schouten, S.; Sinninghe Damsté, J.S. Warm Middle Jurassic–Early Cretaceous high-latitude sea-surface temperatures from the Southern Ocean. *Clim. Past* **2012**, *8*, 215–226. [[CrossRef](#)]
3. Weissert, H.; Mohr, H. Late Jurassic climate and its impact on carbon cycling. *Palaeogeogr. Palaeoclim. Palaeoecol.* **1996**, *122*, 27–43. [[CrossRef](#)]
4. Egyptian General Petroleum Corporation (EGPC). Western Desert, oil and Gas fields, a comprehensive overview. In Proceedings of the EGPC 11th Petroleum Exploration and Production Conference, Cairo, Egypt, 7–10 November 1992; p. 431.
5. Mansour, A.; Geršlova, E.; Sykorova, I.; Vöröš, D. Hydrocarbon potential and depositional paleoenvironment of a Middle Jurassic succession in the Falak-21 well, Shushan Basin, Egypt: Integrated palynological, geochemical and organic petrographic approach. *Int. J. Coal Geol.* **2020**, *219*, 103374. [[CrossRef](#)]
6. El Diasty, W.S.; El Beialy, S.Y.; Littke, R.; Farag, F.A. Source rock evaluation and nature of hydrocarbons in the Khalda Concession, Shushan Basin, Egypt's Western Desert. *Int. J. Coal Geol.* **2016**, *162*, 45–60. [[CrossRef](#)]
7. Gentzis, T.; Carvajal-Ortiz, H.; Deaf, A.S.; Tahoun, S.S. Multi-proxy approach to screen the hydrocarbon potential of the Jurassic succession in the Matruh Basin, North Western Desert, Egypt. *Int. J. Coal Geol.* **2018**, *190*, 29–41. [[CrossRef](#)]
8. Shalaby, M.R.; Hakimi, M.H.; Abdullah, W.H. Modeling of gas generation from the Alam El-Bueib Formation in the Shoushan Basin, northern Western Desert of Egypt. *Int. J. Earth Sci.* **2013**, *102*, 319–332. [[CrossRef](#)]
9. El Nady, M.M.; Mohamed, N.S.; Sharaf, L.M. Geochemical and biomarker characteristics of crude oils and source rock hydrocarbon extracts: An implication to their correlation, depositional environment and maturation in the Northern Western Desert, Egypt. *Egypt. J. Petrol.* **2015**, *25*, 264–268. [[CrossRef](#)]
10. Canfield, D.E. Factors influencing organic carbon preservation in marine sediments. *Chem. Geol.* **1994**, *114*, 315–329. [[CrossRef](#)]
11. Tyson, R.V. Sedimentation rate, dilution, preservation and total organic carbon: Some results of a modeling study. *Org. Geochem.* **2001**, *32*, 333–339. [[CrossRef](#)]
12. Mansour, A.; Wagreich, M.; Gier, S.; Gentzis, T.; Urs, K.; Tahoun, S.S.; Elewa, A.M.T. Climate variability and paleoceanography during the Late Cretaceous: Evidence from palynology, geochemistry and stable isotopes analyses from the southern *Tethys*. *Cret. Res.* **2021**, *126*, 104831. [[CrossRef](#)]
13. Mansour, A.; Wagreich, M. Earth system changes during the cooling greenhouse phase of the Late Cretaceous: Coniacian-Santonian OAE3 subevents and fundamental variations in organic carbon deposition. *Earth-Sci. Rev.* **2022**, *229*, 104022. [[CrossRef](#)]
14. Arndt, S.; Jørgensen, B.B.; LaRowe, D.E.; Middelburg, J.J.; Pancost, R.D.; Regnier, P. Quantifying the degradation of organic matter in marine sediments: A review and synthesis. *Earth-Sci. Rev.* **2013**, *123*, 53–86. [[CrossRef](#)]
15. Said, R. (Ed.) Tectonic framework of Egypt. In *The Geology of Egypt*; Elsevier: Amsterdam, The Netherlands, 1962; pp. 28–44.
16. Meshref, W.M. Tectonic framework. In *The Geology of Egypt*; Said, R., Ed.; Balkema: Rotterdam, The Netherlands, 1990; pp. 113–156.
17. Guiraud, R. Mesozoic rifting and basin inversion along the northern African Tethyan margin: An overview. In *Petroleum Geology of North Africa*; Macgregor, D.S., Moody, R.T., Clark-Lowes, D.D., Eds.; Geological Society: London, UK, 1998; pp. 217–229.
18. Wood, D. The tectonic setting and structural evolution of the Abu Gharadig Basin, western Desert of Egypt. In *Proceedings of the 7th Exploration Seminar*; Egyptian General Petroleum Corporation: Cairo, Egypt, 1986; p. 250.
19. Kerdany, M.T.; Cherif, O.H. Mesozoic. In *The Geology of Egypt*; Said, R., Ed.; Balkema: Rotterdam, The Netherlands, 1990; pp. 407–437.
20. Guiraud, R.; Bellion, Y. Late Carboniferous to Recent geodynamic evolution of the west Gondwanian cratonic Tethyan margins. In *The Ocean Basins and Margins, the Tethys Ocean*; Narin, A.E.M., Ed.; Springer: Boston, MA, USA, 1995; Volume 8, pp. 101–124.
21. Said, R. (Ed.) Cretaceous paleogeographic maps. In *The Geology of Egypt*; Balkema: Rotterdam, The Netherlands, 1990; pp. 439–449.
22. Moustafa, A.R. Mesozoic-Cenozoic Basin Evolution in the Northern Western Desert of Egypt. In Proceedings of the 3rd Symposium on the Sedimentary Basins of Libya (The Geology of East Libya), Benghazi, Libya, 11–13 November 2004; Earth Science Society of Libya: Tripoli, Libya, 2008; Volume 3, pp. 29–46.
23. Müller, G.; Gastner, M. The “Karbonat-Bombe”, a simple device for the determination of the carbonate content in sediments, soils, and other materials. *Neues Jahrb. Mineral. Mon.* **1971**, *10*, 466–469.
24. Tribovillard, N.; Algeo, T.J.; Lyons, T.; Riboulleau, A. Trace metals as paleoredox and paleoproductivity proxies: An update. *Chem. Geol.* **2006**, *232*, 12–32. [[CrossRef](#)]
25. Wedepohl, K.H. The composition of the upper Earth's crust and the natural cycles of selected metals. In *Metals and Their Compounds in the Environment*; Merian, E., Ed.; VCH-Verlagsgesellschaft: Weinheim, Germany, 1991; pp. 3–17.
26. Reitz, A.; Pfeifer, K.; de Lange, G.J.; Klump, J. Biogenic barium and the detrital Ba/Al ratio: A comparison of their direct and indirect determination. *Mar. Geol.* **2004**, *204*, 289–300. [[CrossRef](#)]
27. Schoepfer, S.D.; Shen, J.; Wei, H.; Tyson, R.V.; Ingall, E.; Algeo, T.J. Total organic carbon, organic phosphorus, and biogenic barium fluxes as proxies for paleomarine productivity. *Earth-Sci. Rev.* **2015**, *149*, 23–52. [[CrossRef](#)]
28. Algeo, T.J.; Maynard, J.B. Trace-element behavior and redox facies in core shales of Upper Pennsylvanian Kansas-type cyclothem. *Chem. Geol.* **2004**, *206*, 289–318. [[CrossRef](#)]

29. Ripley, E.M.; Shaffer, N.R.; Gilstrap, M.S. Distribution and geochemical characteristics of metal enrichment in the new Albany shale (Devonian-Mississippian), Indiana. *Econ. Geol.* **1990**, *85*, 1790–2807. [[CrossRef](#)]
30. Berner, R.A.; Raiswell, R. Burial of organic carbon and pyrite sulfur in sediments over Phanerozoic time: A new theory. *Geochim. Cosmochim. Acta* **1983**, *47*, 855–862. [[CrossRef](#)]
31. Lewan, M.D. Factors controlling the proportionality of vanadium to nickel in crude oils. *Geochim. Cosmochim. Acta* **1984**, *48*, 2231–2238. [[CrossRef](#)]
32. Hatch, J.R.; Leventhal, J.S. Relationship between inferred redox potential of the depositional environment and geochemistry of the Upper Pennsylvanian (Missourian) stark shale member of the Dennis Limestone, Wabaunsee County, Kansas, USA. *Chem. Geol.* **1992**, *99*, 65–82. [[CrossRef](#)]
33. Jones, B.; Manning, D.A.C. Comparison of geochemical indices used for the interpretation of palaeoredox conditions in ancient mudstones. *Chem. Geol.* **1994**, *111*, 111–129. [[CrossRef](#)]
34. Zhou, C.; Jiang, S.-Y. Palaeoceanographic redox environments for the lower Cambrian Hetang Formation in South China: Evidence from pyrite framboids, redox sensitive trace elements, and sponge biota occurrence. *Palaeogeogr. Palaeoclimatol. Palaeoecol.* **2009**, *271*, 279–286. [[CrossRef](#)]
35. Ingall, E.; Kolowith, L.; Lyons, T.; Hurtgen, M. Sediment carbon, nitrogen and phosphorus cycling in an anoxic fjord, Effingham Inlet, British Columbia. *Am. J. Sci.* **2005**, *305*, 240–258. [[CrossRef](#)]
36. Mort, H.; Adatte, T.; Föllmi, K.; Steinmann, P.; Matera, V.; Berner, Z.; Stüben, D. Phosphorus and the roles of productivity and nutrient recycling during Oceanic Anoxic Event 2. *Geology* **2007**, *35*, 483–486. [[CrossRef](#)]
37. Babu, C.P.; Brumsack, H.J.; Schnetger, B.; Böttcher, M.E. Barium as a productivity proxy in continental margin sediments: A study from the eastern Arabian sea. *Mar. Geol.* **2002**, *184*, 189–206. [[CrossRef](#)]
38. Rutsch, H.-J.; Mangini, A.; Bonani, G.; Dittrich-Hannen, B.; Kubile, P.W.; Suter, M.; Segl, M. <sup>10</sup>Be and Ba concentrations in western African sediments trace productivity in the past. *Earth Planet. Sci. Lett.* **1995**, *133*, 129–143. [[CrossRef](#)]
39. Kasten, S.; Haese, R.R.; Zabel, M.; Ruhlemann, C.; Schulz, H.D. Barium peaks at glacial terminations in sediments of the equatorial Atlantic Ocean—Relicts of deglacial productivity pulses? *Chem. Geol.* **2001**, *175*, 635–651. [[CrossRef](#)]
40. McManus, J.; Berelson, W.M.; Klinkhammer, G.P.; Johnson, K.S.; Coale, K.H.; Anderson, R.F.; Kumar, N.; Burdige, D.J.; Hammond, D.E.; Brumsack, H.J.; et al. Geochemistry of barium in marine sediments: Implications for its use as a paleoproxy. *Geochim. Cosmochim. Acta* **1998**, *62*, 3453–3473. [[CrossRef](#)]
41. Keeley, M.L.; Dungworth, G.; Floyd, C.S.; Forbes, G.A.; King, C.; McGarva, R.M.; Shaw, D. The Jurassic System in northern Egypt: I. Regional stratigraphy and implications for hydrocarbon prospectively. *J. Pet. Geol.* **1990**, *13*, 397–420. [[CrossRef](#)]
42. El Beialy, S.Y.; Zalat, A.; Ali, A.S. The palynology of the Bathonian-early Oxfordian succession in the East Faghur-1 well, Western Desert, Egypt. *Egypt J. Paleontol.* **2002**, *2*, 399–414.
43. Xia, G.; Mansour, A. Paleoenvironmental changes during the early Toarcian Oceanic Anoxic Event: Insights into organic carbon distribution and controlling mechanisms in the eastern Tethys. *J. Asian Earth Sci.* **2022**, *237*, 105344. [[CrossRef](#)]
44. Liguori, B.T.P.; Almeida, M.G.D.E.; Redenze, C.E.D.E. Barium and its Importance as an Indicator of (Paleo)Productivity. *An. Acad. Bras. Ciênc.* **2016**, *88*, 2093–2103. [[CrossRef](#)]
45. Ratcliffe, K.T.; Wright, A.M.; Spain, D.R. Unconventional methods for unconventional plays: Using elemental data to understand shale resource plays. *Pet. Explor. Soc. Aust. News Res.* **2012**, *117*, 50–54.
46. Taylor, S.R.; McLennan, S.M. *The Continental Crust: Its Composition and Evolution*; Blackwell: Malden, MA, USA, 1985.
47. Chen, H.-F.; Yeh, P.-Y.; Song, S.-R.; Hsu, S.-C.; Yang, T.-N.; Wang, Y.; Chi, Z.; Lee, T.-Q.; Chen, M.-T.; Cheng, C.-L.; et al. The Ti/Al molar ratio as a new proxy for tracing sediment transportation processes and its application in aeolian events and sea level change in East Asia. *J. Asian Earth Sci.* **2013**, *73*, 31–38. [[CrossRef](#)]
48. Ratcliffe, K.T.; Wright, A.M.; Hallsworth, C.; Morton, A.; Zaitlin, B.A.; Potocki, D.; Wray, D. An example of alternative correlation techniques in a low-accommodation setting, nonmarine hydrocarbon system: The (Lower Cretaceous) Mannville Basal Quartz succession of southern Alberta. *Am. Assoc. Pet. Geol. Bull.* **2004**, *88*, 1419–1432. [[CrossRef](#)]
49. LaGrange, M.T.; Konhauser, K.O.; Catuneanu, O.; Harris, B.S.; Playter, T.L.; Gingras, M.K. Sequence stratigraphy in organic-rich marine mudstone successions using chemostratigraphic datasets. *Earth-Sci. Rev.* **2020**, *203*, 103137. [[CrossRef](#)]
50. Fralick, P.W.; Kronberg, B.I. Geochemical discrimination of clastic sedimentary rock sources. *Sediment. Geol.* **1997**, *113*, 111–124. [[CrossRef](#)]
51. Schlanger, S.O. Strontium storage and release during deposition and diagenesis of marine carbonates release to sea-level variations. In *Physical and Chemical Weathering in Geochemical Cycles*; Lerman, A., Meybeck, M., Eds.; Kluwer Academic: Dordrecht, The Netherlands, 1988; pp. 323–339.
52. Dypvik, H.; Harris, N.B. Geochemical facies analysis of fine-grained siliciclastics using Th/U, Zr/Rb and (Zr + Rb)/Sr ratios. *Chem. Geol.* **2001**, *181*, 131–146. [[CrossRef](#)]
53. Fourcade, E.; Azéma, J.; Bassoulet, J.-P.; Cecca, F.; Dercourt, J.; Enay, R.; Guiraud, R. Paleogeography and Paleoenvironment of the Tethyan Realm During the Jurassic Breakup of Pangea. In *The Tethys Ocean*; Nairn, A.E.M., Ricou, L.E., Vrielynck, B., Dercourt, J., Eds.; Springer: Boston, MA, USA, 1995. [[CrossRef](#)]
54. McLennan, S.M.; Hemming, S.; McDaniel, D.K.; Hanson, G.N. Geochemical approaches to sedimentation, provenance, and tectonics. *Geol. Soc. Am. Spec. Pap.* **1993**, *284*, 21–40.

55. Bouchez, J.; Gaillardet, J. How accurate are rivers as gauges of chemical denudation of the Earth surface? *Geology* **2014**, *42*, 171–174. [[CrossRef](#)]
56. Dellinger, M.; Gaillardet, J.; Bouchez, J.; Calmels, D.; Louvat, P.; Dosseto, A.; Gorge, C.; Alanoca, L.; Maurice, L. Riverine Li isotope fractionation in the Amazon River basin controlled by the weathering regimes. *Geochim. Cosmochim. Acta* **2015**, *164*, 71–93. [[CrossRef](#)]
57. Niebuhr, B. Geochemistry and time-series analyses of orbitally forced Upper Cretaceous marl-limestone rhythmites (Lehrte West Syncline, northern Germany). *Geol. Mag.* **2005**, *142*, 31–55. [[CrossRef](#)]
58. Shen, J.; Zhang, E.L.; Xia, W.L. Records from lake sediments of the Qinghai lake to mirror climatic and environmental changes of the past about 1000 years. *Quat. Res.* **2001**, *21*, 508–513.
59. Zobia, M.K.; El Beialy, S.Y.; El-Sheikh, H.A.; El Beshtawy, M.K. Jurassic-Cretaceous palynomorphs, palynofacies, and petroleum potential of the Sharib-1X and Ghoroud-1X wells, north Western Desert, Egypt. *J. Afr. Earth Sci.* **2013**, *78*, 51–65. [[CrossRef](#)]
60. Ricken, W. Bedding rhythms and cyclic sequences as documented in organic carbon-carbonate patterns, Upper Cretaceous, Western Interior, U.S. *Sediment. Geol.* **1996**, *102*, 131–154. [[CrossRef](#)]
61. Pratt, L.M. Influence of palaeoenvironmental factors on the preservation of organic matter in middle Cretaceous Greenhorn Formation near Pueblo, Colorado. *AAPG Bull.* **1984**, *68*, 1146–1159.
62. Meyers, S.R.; Sageman, B.B.; Lyons, T.W. Organic carbon burial rate and the molybdenum proxy: Theoretical framework and application to Cenomanian-Turonian oceanic anoxic event 2. *Paleoceanography* **2005**, *20*, PA2002. [[CrossRef](#)]
63. Kennedy, M.J.; Wagner, T. A clay mineral continental amplifier for marine carbon sequestration in a greenhouse ocean. *Proc. Natl. Acad. Sci. USA* **2011**, *108*, 9776–9781. [[CrossRef](#)]
64. Henrichs, S.M.; Reeburgh, W.S. Anaerobic mineralization of marine sediment organic matter: Rates and the role of anaerobic processes in the oceanic carbon economy. *Geomicrobiol. J.* **1987**, *5*, 191–237. [[CrossRef](#)]